Heavy Flavour Spectroscopy

Rob Kutschke
University of California, Santa Barbara

Abstract

It is now almost 20 years since the discovery of hadrons with open charm and, over this period, more than 20 charmed mesons and baryons have been established. Moreover some striking patterns have been observed in the strong and electromagnetic transitions between these states. In these lectures, the status of both the theoretical and the experimental knowledge of charm spectroscopy and decays will be reviewed. It has also been about 10 years since the discovery of hadrons with open b quantum numbers. While this spectroscopy is still in its infancy, it will also be discussed.

Lectures presented at the NATO Advanced Study Institute on Hadron Spectroscopy and the Confinement Problem. London and Swansea, July 1995.

1 Introduction

During the first week of this institute many people expressed some wonder that four lectures had been allotted to discuss the spectroscopy of hadrons with heavy flavour. Surely there are simply not enough such hadrons to warrant a full four hours! A glance at figures 1 and 2, however, should reassure any doubters. Figure 1a) shows the measured mass spectrum of all of the known charmed mesons, while part b) shows the same for of all of the known charmed baryons and figure 2 shows the same for all known bottom mesons. The quark content of the various states named in these figures is summarized in Tables 1 and 2. At this time the only established bottom baryon is the Λ_b, so there is no corresponding figure for the bottom baryons.[1] Because most of the known states are charmed hadrons, this review will mostly cover charm spectroscopy, with a few references to bottom spectroscopy. Finally, whenever these lectures discuss a particular state or reaction, the charge conjugate state or reaction is usually implied. The exceptions will occur when discussing charm production from Σ^- beams or $\overline{\nu}$ beams.

These lectures are organized as follows. They will begin with a short section on naming conventions followed by an overview of the decay modes in which the various excited states are seen. This will also serve as a guide to where the most interesting parts of the main discussion will be. The main section will be a survey of the theory, with frequent asides to compare with data. After that will come a discussion of experimental techniques and, finally, a presentation of some experimental results which did not find a home in the main section. Because the field is now over 20 years old, many of the elementary results have long been "assumed knowledge" and are rarely discussed, even in modern textbooks. These proceedings provide an opportunity to remind people of many of these results, which often boil down to nothing more than conservation of angular momentum or elementary quantum mechanics.

[1] Over the summer several LEP experiments have shown evidence for several new bottom hadrons, however the author has not yet had time to digest this new information and it will not be presented here

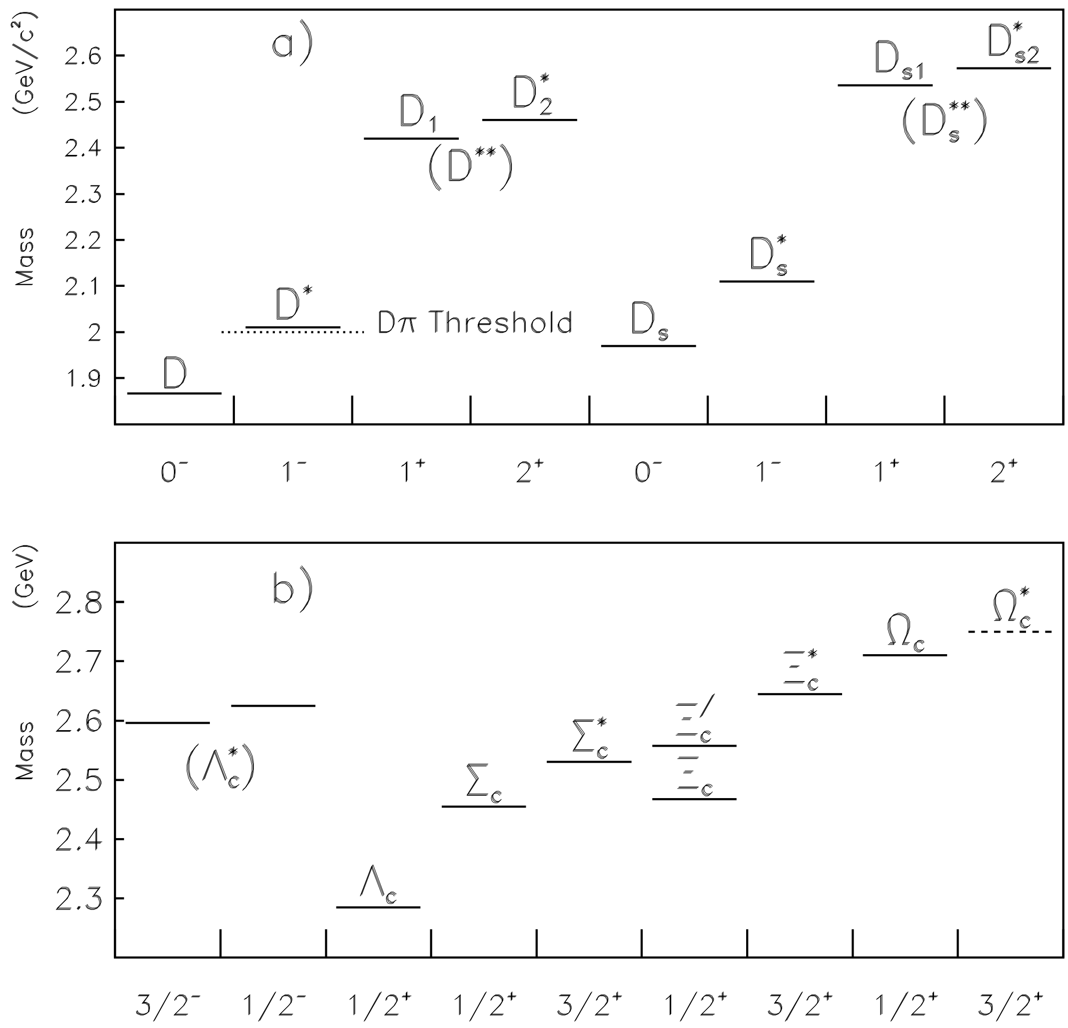

Figure 1: Measured mass spectrum of the known charmed (a) mesons and (b) baryons. The horizontal axis indicates the spin and parity, J^P, of the state. In most cases, the J^P is a theoretically motivated assignment, not the result of a measurement. There is one undiscovered member in the spatial ground state of the singly charmed baryons, the Ω_c^*; the predicted mass for this state is indicated with a dashed line. The Ξ_c^* and the Σ_c^* multiplets are incomplete, with only the Σ_c^{*++} and Ξ_c^{*0} having been observed. The names given in brackets are not official nomenclature but are frequently used. The formal names of the two excited Λ_c states shown to the left of part (b) are the $\Lambda_c(2593)$ and the $\Lambda_c(2625)$. In part (a) the $D\pi$ threshold is shown as a dotted line. The data are taken from [1](D_s^*), [2](D^{**}, D_s^{**}), [3](Ξ_c^*), [4](Ω_c), [5](Λ_c^*), and the remaining data are taken from [6]. The errors on the masses are small compared to the line thickness.

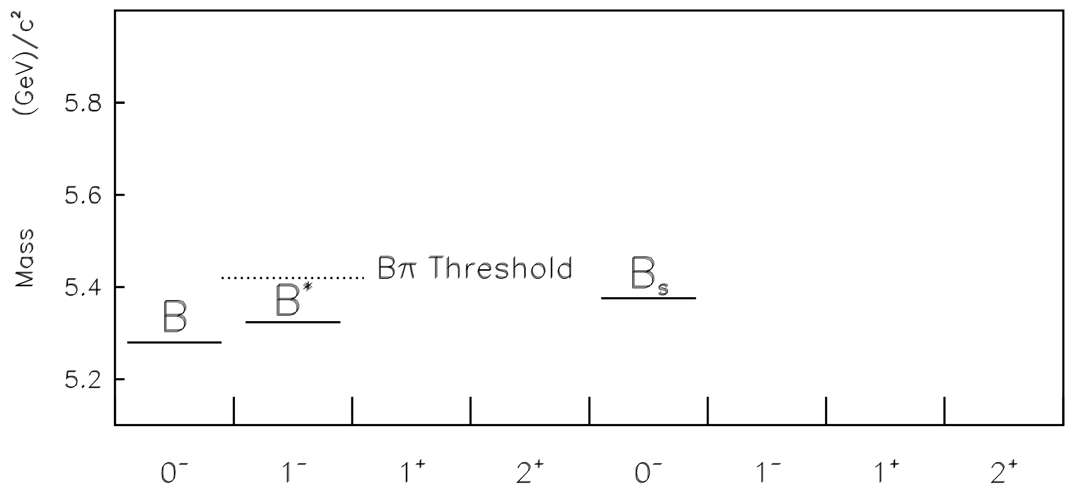

Figure 2: Mass spectrum of the known mesons which contain a b quark. The vertical scale is the same as that used in Figure 1. Note that, unlike in the charm sector, the first excitation lies below the threshold for decay to $B\pi$. No corresponding figure has been made for the b baryon sector because only one state is known, the Λ_b, at a mass of $5641. \pm 50.$ MeV$/c^2$. The data are taken from [6].

2 Overview of Names and Decays

2.1 Taxonomy

The subset of heavy flavour mesons considered in these lectures will be those that consist of either a charmed quark, c, or a bottom quark, b, bound together with a light anti-quark, $\overline{q}$, where $q = u, d, s$. That is, states such as $b\overline{c}$, for which there are no experimental data, will not be discussed. When it is not important to distinguish between charm and bottom mesons the notation $Q\overline{q}$ will be used, where Q denotes a heavy quark. On occasion the notation q will refer only to the u and d quarks, but not to s; such instances will be clearly noted.

The naming scheme for the hadrons, described in the Review of Particle Properties[6], allows one to determine the quark content of a heavy flavour meson directly from its name. This correspondence between meson name and quark content is summarized, for the ground state mesons, in Table 1. The unadorned symbol D is often used when it is not important to make

Quark Content	Name	Quark Content	Name
$c\overline{u}$	D^0	$\overline{b}u$	B^+
$c\overline{d}$	D^+	$\overline{b}d$	B^0
$c\overline{s}$	D_s^+	$\overline{b}s$	B_s^0
		$\overline{b}c$	B_c^+
$\overline{c}u$	$\overline{D}^0$	$b\overline{u}$	B^-
$\overline{c}d$	D^-	$b\overline{d}$	$\overline{B}^0$
$\overline{c}s$	D_s^-	$b\overline{s}$	$\overline{B}_s^0$
		$b\overline{c}$	B_c^-

Table 1: Quark content of the ground state charmed and bottom mesons. The nomenclature for excited states is summarized in table 6. Because it is redundant, the charge superscript on the strange mesons is often dropped.

distinctions between the D^+ and the D^0, while an undifferentiated anti-charm meson is denoted as $\overline{D}$. Similarly, for the symbols B and $\overline{B}$.

Notice the convention that a $c\overline{q}$ system is a particle, D, whereas a $b\overline{q}$ system is an anti-particle, $\overline{B}$. This sign convention was chosen for a variety of reasons, one of which is that all flavours carried by a charged meson have the same sign as the charge of the meson. For example, the D_s^+ has both charm and strangeness of $+1$. A second reason is that all particles have semileptonic decays to $e^+\nu_e$ whereas as anti-particles have semileptonic decays to $e^-\overline{\nu_e}$.

The Particle Data Group (PDG) naming scheme for hadrons also allows one to extract the quark content of a baryon from its name. This correspondence between the name of a baryon and its quark content is summarized in Table 2. Following the example of mesons, the symbol, Σ_c for example, is used to denote an unspecified member of the Σ_c multiplet and the symbol $\overline{\Sigma}_c$ is used to denote an unspecified member of the anti-baryon multiplet.

Recall that the distinction between the Λ and the Σ^0, both of which have quark content sud, is that the Λ has isospin $I = 0$ whereas the Σ is the $I_3 = 0$ member of an $I = 1$ multiplet. All other differences between these two baryons, such as the spin of the ud diquark, are derived from this fundamental difference. This same distinction carries over into the charmed sector.

Quarks	I	Nomenclature	Quarks	I	Nomenclature
cud	0	Λ_c	bud	0	Λ_b
cuu, cud, cdd	1	$\Sigma_c^{++}, \Sigma_c^{+}, \Sigma_c^{0}$	buu, bud, bdd	1	$\Sigma_b^{+}, \Sigma_b^{0}, \Sigma_b^{-}$
csu, csd	$\frac{1}{2}$	Ξ_c^{+}, Ξ_c^{0}	bsu, bsd	$\frac{1}{2}$	Ξ_b^{0}, Ξ_b^{-}
css	0	Ω_c	bss	0	Ω_b
ccu, ccd	$\frac{1}{2}$	$\Xi_{cc}^{++}, \Xi_{cc}^{+}$	bbu, bbd	$\frac{1}{2}$	$\Xi_{bb}^{0}, \Xi_{bb}^{-}$
ccs	0	Ω_{cc}	bbs	0	Ω_{bb}
ccc	0	Ω_{ccc}	bbb	0	Ω_{bbb}
			bcs	0	Ω_{bc}
			bcc	0	Ω_{bcc}
			bbc	0	Ω_{bbc}

Table 2: Quark content of the ground state charmed and bottom baryons. The column headed I denotes the isospin of the baryon. The nomenclature of excited states, which are denoted by adding a variety of superscripts to the base name, will be discussed in sections 3.2.1 and 3.2.2. A cross-reference between these names and a naming convention used in some older papers is found in table 3.

PDG Name	Old Name	PDG Name	Old Name	PDG Name	Old Name
Λ_c	C_0	Σ_c	C_1	Ξ_c	A
Ξ_c'	S	Ξ_c^*	S^*	Ω_c	T
Ω_c^*	T^*	Ξ_{cc}	X_u, X_d	Ω_{cc}	X_s

Table 3: Correspondence between Particle Data Group baryon names and a scheme used in some older papers [7].

Decay	Branching Fraction (%)	$Q(MeV)$
$D^{*+} \to D^+\gamma$	$1.1 \pm 1.4 \pm 1.6$	
$D^{*+} \to D^+\pi^0$	$30.8 \pm 0.4 \pm 0.8$	5.66 ± 0.09
$D^{*+} \to D^0\pi^+$	$68.1 \pm 1.0 \pm 1.3$	5.85 ± 0.05
$D^{*0} \to D^0\gamma$	$36.4 \pm 2.3 \pm 3.3$	
$D^{*0} \to D^0\pi^0$	$63.6 \pm 2.3 \pm 3.3$	7.14 ± 0.07
$D^{*0} \to D^+\pi^-$	kinematically forbidden	

Table 4: The D^* branching ratios from [8]. For the strong decays, the Q value of the decay is also given. The first row of the table corresponds to the upper limit, $B(D^{*+} \to D^+\gamma) \leq 4.2\%$ @ 90% C.L.

2.2 Overview of Decays

This section summarizes the allowed transitions among the states in figures 1 and 2. The following states only decay weakly and their decays will not be discussed in these lectures: D^0, D^+, D_s, B^0, B^-, B_s, Λ_c, Ξ_c and Ω_c. As will be discussed in section 3.2.1, it is interesting that the Σ_c is absent from this list. The following states are below threshold to decay via π emission and have been observed to decay electromagnetically: B^{*-}, B^{*0} and Ξ_c'. It is expected that the unobserved Ω_c^* will also only decay electromagnetically.

While the D_s^* is above threshold to decay to $D_s\pi^0$, that decay violates isospin and it was believed that the D_s^* only decayed electromagnetically. However, because isospin is not an exact symmetry the decay $D_s^* \to D_s\pi^0$ is merely suppressed, not forbidden, and it has recently been observed.

Because the D^* states are so close to the $D\pi$ threshold, their strong decay widths are severely limited by phase space and the electromagnetic decay $D^{*0} \to D^0\gamma$ has a rather large branching fraction, about 36%. For many years it was thought that $B(D^{*+} \to D^+\gamma)$ was approximately 15% however it is now known to be less than 4.2% at 90% C.L.. In this case the theorists insisted that they had to be right and that the experiments were wrong. They were right, and their simple argument is sketched in section 3.4. The story of the strong decays of the D^* mesons is dominated by their small Q values, which are listed in table 4.

The remaining states decay only strongly. The D^{**} states decay to $D\pi$ and $D^*\pi$, while the D_s^{**} states decay to DK and D^*K. The Σ_c and Σ_c^* both decay to $\Lambda_c\pi$, while the Ξ_c^* decays to $\Xi_c\pi$. This leaves the Λ_c^* states, which decay to $\Lambda_c\pi\pi$, but not to $\Lambda_c\pi$. As is discussed in section 3.2.2, the absence the $\Lambda_c\pi$ decay mode which suggests the classification of these states as Λ_c excitations, not Σ_c excitations.

3 Theory, with many Experimental Asides

3.1 Heavy Flavour Mesons

While it is generally believed that QCD is the correct fundamental theory of the strong interactions there are, as yet, no practical means to produce full QCD calculations of hadron masses and their decay widths. In order to get around this problem a variety of different approximate methods have been tried, among them lattice calculations, QCD sum rules, the Bag Model and potential models. The last of these has proved to be the most useful in understanding the mass spectrum and the decay patterns of heavy flavour hadrons. Moreover many of its predictions can be expressed in simple closed forms, rather than in vast tables of numbers. Therefore these proceedings will discuss the data in terms of potential models. The simplest of these is the Non-relativistic Quark Potential Model (NRQPM), for which useful reviews can be found in [9] and [10].

Shortly after the discovery of the J/ψ the properties of the charmed mesons and baryons were predicted by the use of a potential model [11]. While the details of modern potential models have evolved a great deal, the essential features remain unchanged. The most important features are that the inter-quark potential has two distinct regimes: at short distances the potential is dominated by a one gluon exchange term, proportional to $1/r$, while, at large distances it is dominated by a confining potential which is proportional to r and which comes from an effective scalar exchange. Here r is the inter-quark separation. Another important feature is that, except for mass dependences, the inter-quark potential is independent of quark flavour. Reference [12] provides a review of what has been learned about the inter-quark potential by studies of $Q\overline{Q}$ mesons.

While the above features have not been formally derived from QCD, they are certainly motivated by QCD. In an asymptotically free theory, such as QCD, the short distance behaviour should be dominated by lowest order perturbation theory, that is, by one gluon exchange. The linear behaviour at large r can be seen by considering a thought experiment in which a $q\overline{q}$ pair are held apart by an external force. Because gluons carry colour charge, they are attracted to each other and the colour field lines, instead of looking like an electromagnetic dipole field, lie in a narrow cylinder along the line which joins the $q\overline{q}$ pair. It is said that a colour flux tube forms between the pair. Lattice calculations suggest that the tension per unit length in this flux tube is a constant [13][14]. Therefore the energy stored in the flux tube is proportional to the separation of the charges. Finally, because the underlying gauge theory, QCD, has flavour independent couplings, the effective theory does too.

The strongest experimental evidence that the long distance part of the potential is due to an effective scalar exchange comes from the recent observation of the h_c. The mass of this meson is within about 1 MeV of the spin weighted center-of-mass of the χ_c multiplet. In a model with effective scalar exchange at long distances this state should be degenerate with the spin weighted center-of-mass of the χ_c multiplet. On the other hand, an effective vector exchange would give rise to a splitting on the order of several tens of MeV [15].

The various potential models which have been advanced all roughly follow the above picture. Most differences fall into two categories: one is the limiting behaviour at large r, is it exactly linear or only approximately linear. The second class of differences concern the details of the shape at intermediate values of r, a range in which the potential is not well constrained by the available data. Most of the data lies either at large r (π and ρ) or at small r (Υ). It is expected that the excited charm states will provide more data in this region.

The most complete potential model, one which describes the mass spectrum and decays of all hadrons from the π to the Υ, is that developed by Godfrey and Isgur [16] for mesons and by Capstick and Isgur for baryons[17]. They start with a non-relativistic potential model and add some of the consequences of relativity by hand. Their method changes the parameterization of the wavefunctions and the details of some of the decays. Because they do not perform a full relativistic treatment their model is said to be "relativized", rather than relativistic. The following will sketch their model for mesons using a notation which is a mixture of that from [16] and that from [18]. The model for baryons will be discussed in section 3.2

The Hamiltonian of the Godfrey-Isgur model is written in terms of the inter-quark separation, $\vec{r} = \vec{r}_1 - \vec{r}_2$, and its conjugate momentum, $\vec{p} = \vec{p}_1 - \vec{p}_2$. Here the labels 1 and 2 refer to the quark and anti-quark which make up the meson. Other notation that is needed are the masses and spins of the quarks, m_i and $\vec{S}_i$, the orbital angular momentum between the quarks $\vec{L}$, the total spin of the quarks, $\vec{S} = \vec{S}_1 + \vec{S}_2$, and the total angular momentum of the meson, $\vec{J} = \vec{S}_1 + \vec{S}_2 + \vec{L}$. Finally, $r = |\vec{r}|$ and $p = |\vec{p}|$. The Hamiltonian has the form,

$$H = H_0 + H_c + H_{BF}, \tag{1}$$

where the subscripts denote the free Hamiltonian (H_0), the confinement part of the Hamiltonian (H_c) and a spin dependent part which is reminiscent of the Breit-Fermi Hamiltonian of atomic and nuclear physics (H_{BF}). Written in full, these pieces are,

$$\begin{aligned} H_0 &= m_1 + \frac{p^2}{2m_1} + m_2 + \frac{p^2}{2m_2} \\ H_c &= -\frac{4}{3}\frac{\alpha_s}{r} + a + br \\ H_{BF} &= c_1\vec{L}\cdot\vec{S}_1 + c_2\vec{L}\cdot\vec{S}_2 + c_T\left(3\vec{S}_1\cdot\hat{r}\vec{S}_2\cdot\hat{r} - \vec{S}_1\cdot\vec{S}_2\right) + c_H\vec{S}_1\cdot\vec{S}_2, \end{aligned} \tag{2}$$

where,

$$\begin{aligned} c_i &= \left(\frac{1}{m_i^2} + \frac{1}{m_1 m_2}\right)\frac{4}{3}\frac{\alpha_s}{r^3} - \frac{1}{2m_i^2}\frac{b}{r} \\ c_T &= \frac{1}{m_1 m_2}\frac{4}{3}\frac{\alpha_s}{r^3} \\ c_H &= \frac{8\pi}{3}\frac{1}{m_1 m_2}\frac{4}{3}\frac{\alpha_s}{r}\delta^3(\vec{r}). \end{aligned} \tag{3}$$

In the above there is one crucial sign, which is a prediction of the model — the negative sign between the α_s and the b contributions to the spin-orbit coupling. While each of these contributions is large compared to the spin-spin coupling, the two contributions cancel almost exactly. In the light baryon sector, this cancelation explains the unexpected success of the original Isgur-Karl model[19], in which the spin-orbit terms were simply ignored!

It is important to point out that, in the relativized quark potential model, most of the parameters were determined from the light hadrons, charmonium and bottomonium. This model, therefore, makes actual predictions for most of heavy flavour spectroscopy and decays.

The last part of the model is to specify the constituent masses of the quarks. Typical values used in non-relativistic models are $m_u = m_d = 350$ MeV, $m_s = 550$ MeV, $m_c = 1500$ MeV and $m_b = 5000$ MeV. In the relativized model of Godfrey and Isgur the masses used are, $(m_u + m_d)/2 = 220$ MeV, $m_s = 419$ MeV, $m_c = 1628$ MeV and $m_b = 4977$ MeV. These two models also have slightly different values for a and b.

3.1.1 A Reminder about $Q\overline{Q}$ and $q\overline{q}$

First, consider the predictions of this Hamiltonian for the mass spectra of the $c\overline{c}$ and $b\overline{b}$ systems. Because of angular momentum conservation and parity conservation, the quantum numbers J^P must be good quantum numbers of the eigenstates of this Hamiltonian. Further, the constituents turn into each other under charge conjugation, C. Also, QCD conserves C and I. Therefore the complete set of observable quantum numbers for the eigenstates of this system is IJ^{PC}. Because P and C are good quantum numbers, S must also be a good quantum number. Within the context of quark potential models one should also consider the quantum number L. Even though L, is not a good quantum number, it is useful to start in a basis with definite L and to treat mixing between states of the same J^{PC} but different L as a perturbation. States with definite L and S are denoted by the spectroscopic notation ${}^{2S+1}L_J$ and they have the well known properties, $P = (-1)^{L+1}$ and $C = (-1)^{L+S}$. A list of these states, sorted by J^{PC} is summarized in Table 5. When two spectroscopic states give rise to the same J^{PC}, the physical states will be mixtures of these two states. Therefore the physical states with, for example, $J^{PC} = 1^{--}$, will be a mixture of ${}^3S_1$ and ${}^3D_1$. Also, all states of a given J^P have the same S — this is just the statement that S is a good quantum number.

Recall that the specific example being discussed is the mass spectra of charmonium and bottomonium. In these systems the multiplets of given L are separated from each other by several hundred MeV while the states within the multiplets have widths of, at most, a few MeV. Recall that perturbation theory suppresses the mixing of such states with large energy difference denominators. The lowest lying 1^{--} meson will, therefore, be almost pure ${}^3S_1$, with only a small ${}^3D_1$ component. This example illustrates that, although

J	PC			
	$-+$	$+-$	$--$	$++$
4	$^1G_4$		$^3G_4$	$^3F_4,\ ^3H_4$
3		$^1F_3$	$^3D_3,\ ^3G_3$	$^3F_3$
2	$^1D_2$		$^3D_2$	$^3P_2,\ ^3F_2$
1		$^1P_1$	$^3S_1,\ ^3D_1$	$^3P_1$
0	$^1S_0$			$^3P_0$

Table 5: Quantum numbers J^{PC} for quark model meson states of specific $^{2S+1}L_J$.

L is not formally a good quantum number, there are cases in which it is effectively a good one. It is therefore meaningful to speak of things such as S-wave mesons and P-wave mesons, which have $L = 0$ and $L = 1$, respectively. On the other hand this will not work for all cases. It may happen that, for example, a radial excitation of the $^3S_1$ configuration lies close enough to the $^3D_1$ that the physical states will have significant mixing.

In systems containing only u and d quarks, C is no longer (except for the neutral states) a good quantum number but G parity is good. The above arguments can all be repeated with G replacing C and most of the same results are obtained. The only significant difference is that, because some of the states are broad, more care must be taken when discussing the mixing between the two spectroscopic states which contribute to a given J^{PC}.

3.1.2 The Quantum numbers of $Q\overline{q}$

In order to apply quark potential models to hadrons containing heavy flavours one must first consider how $Q\overline{q}$ mesons differ from the $Q\overline{Q}$ and $q\overline{q}$ mesons. The most important difference is that, because neither C nor G are good quantum numbers, S is no longer a good quantum number. An exception is that for mesons with $L = 0$, $S = J$ and, because J is a good quantum number, so is S.

On the other hand, the limit of the potential model Hamiltonian as $m_Q \to \infty$ is particularly simple,

$$H = m_Q + m_q + \frac{p^2}{2m_q} - \frac{4}{3}\frac{\alpha_s}{r} + a + br$$

$$+\frac{1}{m_q^2}\left(\frac{4}{3}\frac{\alpha_s}{r^3}-\frac{1}{2}\frac{b}{r}\right)\vec{L}\cdot\vec{S}_q. \tag{4}$$

This Hamiltonian has a new good quantum number which is present only in this limit and not in the general Hamiltonian. The new quantum number is the total angular momentum of the light quark,

$$\vec{j}_\ell \;=\; \vec{S}_q+\vec{L}. \tag{5}$$

As will be discussed at the end of this section, j_ℓ is usually known as the total angular momentum of the "light degrees of freedom" and it has a direct analogy with the total angular momentum of an electron in a hydrogen atom. It is because of this that heavy-light mesons are often referred to as the "hydrogen atom of QCD"[18].

For mesons with $L=0$, $S=J$, and working in the $m_Q\to\infty$ limit leads to the same spectroscopy as does the full Hamiltonian, a ${}^1S_0$ state and a ${}^3S_1$ state. When L is non-zero, however, there is a question of how to the couple the three angular momenta in the problem. For example, one could couple the angular momenta as $\vec{J}=(\vec{S_Q}+\vec{S_q})+\vec{L}$ or as $\vec{J}=\vec{S_Q}+(\vec{S_q}+\vec{L})$. While the final physics must not depend on the order of coupling, a poor choice can lead to a large increase in the amount of algebra required to reach the final answer. In the case that S is a good quantum number, the physical states will be obtained directly by coupling the angular momenta as $\vec{J}=(\vec{S_Q}+\vec{S_q})+\vec{L}$. On the other hand, in the limit that $m_Q\to\infty$, the physical states will be obtained directly by coupling the angular momenta as $\vec{J}=\vec{S_Q}+(\vec{S_q}+\vec{L})$. When neither case is appropriate one must do perturbation theory about one of these choices.

Figure 3 shows an example of the different coupling schemes for the $c\overline{q}$ mesons in the case that $L=1$. The spin weighted center-of-mass of the P-wave mesons is shown at the left of the figure and is denoted by the label P. In the limit that $m_Q\to\infty$, this multiplet splits into a doublet in which the members have $j_\ell=3/2$ and $j_\ell=1/2$. These states are denoted by the spectroscopic notation $L^{j_\ell P}$. Notice that the spin weighted center-of-mass is preserved by this splitting. When one sets $m_Q=m_c$, each of these states splits into a doublet, leading to a final pattern of a doublet of doublets. These states are labeled using a spectroscopic notation of $L_J^{j_\ell P}$. For comparison, the right half of the figure shows what the splitting would be like if the pattern of the charmonium splitting were reproduced. For this figure, the ${}^3P_2-{}^3P_0$

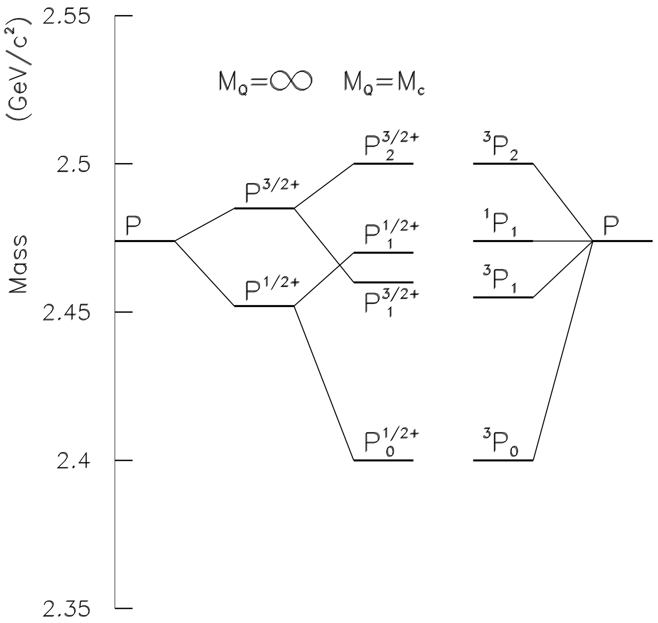

Figure 3: Splittings within the P-wave charm multiplet, following the predictions of [20]. See the discussion in the text for details.

splitting was fixed to that found on the left half of the figure. While the differences between the mass spectra on the left and right sides of this figure are not dramatic, it will be seen in section 3.3 that the differences in the decay patterns are.

There is one feature missing from the discussion presented above. Because the charmed quark mass is not infinite, only large, j_ℓ is not a good quantum number and $P_1^{3/2+}$ state can mix with the $P_1^{1/2+}$ state, either through the spin dependent parts of the Hamiltonian or through their common decay channels.

The masses used in drawing this figure were obtained from [20], who predict that $M(P_1^{1/2+}) > M(P_1^{3/2+})$. Other authors, however, predict that the opposite will be true. That is, there is no agreement among theorists as to whether or not the doublets cross over. While this calculation does not include decay channel mixing, it does include all other effects, including the finite value of m_c. Most other authors present their results in either the $m_c \to \infty$ limit or in the ${}^3P_1$-${}^1P_1$ limit and do not make an attempt to calculate the deviations from the limit. This is one of the reasons that these proceedings focus on the model of [20, 16, 17].

Candidates for the first charmed [21] and charmed-strange [22] P-wave mesons were first observed by ARGUS. Since then, all of the $c\overline{q}$ states and $c\overline{s}$ states with $j_\ell = 3/2$ have been observed and the predictions presented here are in reasonable agreement with the experimental results. Most of the modern potential models predict the intra-multiplet splittings to within about 10 MeV of the measured values and the inter-multiplet splittings to within about 40 MeV. An extensive review article on P-wave charmed mesons has been accepted for publication [2] and some of the world averages computed in that review will be discussed in section 5.3.

Now that the necessary spectroscopic notation has been defined, it is possible to complete the discussion on meson naming conventions which was begun in table 1. Table 6 continues that table to include some of the excited charmed states. Following the Particle Data Group conventions, the vector mesons are denoted by adding a superscript * to the base name. All of the remaining excited states have a subscript denoting the spin of the meson. Those excited states from the natural J^P series, $0^+, 1^-, 2^+ \ldots$, also have a superscript *. Those from the unnatural J^P series, $0^-, 1^+, 2^- \ldots$, do not have a superscript *. Any remaining confusion is separated by adding the value of

Quark Content	Notation	S − wave		P − wave	
	J^P	0^-	1^-	2^+	1^+
	${}^{2S+1}L_J$	${}^1S_0$	${}^3S_1$		
	$L_J^{j_\ell}$	$S_0^{\frac{1}{2}}$	$S_1^{\frac{1}{2}}$	$P_2^{\frac{3}{2}}$	$P_1^{\frac{3}{2}}$
$c\overline{u}$		D^0	D^{*0}	D_2^{*0}	D_1^0
$c\overline{d}$		D^+	D^{*+}	D_2^{*+}	D_1^+
$c\overline{s}$		D_s^+	D_s^{*+}	D_{s2}^{*+}	D_{s1}^+

Table 6: Correspondence between quark content, angular momentum quantum numbers and meson name for the known charmed mesons.

the mass to the name. For example, the $P_1^{3/2+}$ $c\overline{u}$ state is well established, has a mass of about 2420 MeV, and is known as the $D_1(2420)^0$. When discovered, its $P_1^{1/2+}$ partner will be known as the $D_1(M)^0$, where M is the mass of the state. Because j_ℓ is only approximately a good quantum number, the Particle Data Group naming scheme does not include that information.

The Particle Data Group [6] refers to a state called the $D_J(2440)^+$, where J indicates that the spin is unknown. This state was seen using a partial reconstruction technique [23] which was only able to obtain large errors on the mass. The state lies within one standard deviation of the mass of the $D_1(2420)^0$, as determined by the same experiment, and it has always been understood to be the isospin partner of the $D_1(2420)^0$. Now that the $D_1(2420)^+$ has been firmly established [24], at a mass of $2425\pm2\pm2$ MeV, the $D_J(2440)^+$ should be renamed the $D_1(2420)^+$.

Finally, figure 4 shows the predicted invariant mass spectrum from [16] and [20] for many states in the charmed non-strange sector. Because the separation from the F-wave states is about 500 MeV, the lowest lying P-wave states should have very little F wave admixture. In this model the overall mass scale in this sector is about 20 MeV too high but the model otherwise describes the data well.

The above discussion is the first exposure in these lectures to a simple but important idea which, over the past 6 or 7 years, has transformed the theory of hadrons with heavy flavour, Heavy Quark Effective Theory (HQET)[25, 26]. In the limit that $m_Q \to \infty$, QCD has an exact symmetry that the mass

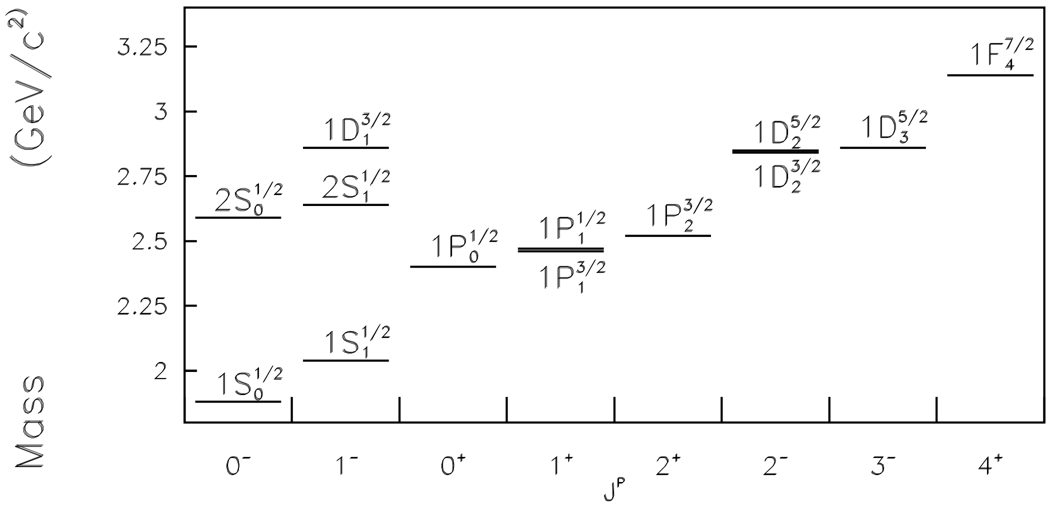

Figure 4: Mass spectrum of charmed meson predicted by the model of Godfrey and Isgur [16], [20].

and the spin of the heavy quark completely decouple from all dynamics. The preceding discussion shows how this occurs in a potential model but the result is also true in the full theory. Motivated by this idea, one says that as $m_Q \to \infty$, the quantum numbers of a $Q\overline{q}$ meson are just those of the "light degrees of freedom". In a constituent quark model the light degrees of freedom are simply those of the light quark. In full QCD the light degrees of freedom are the sum of a current light quark, along with its associated virtual gluons and $q\overline{q}$ pairs. A third example concerns the decay of an excited charm meson to $D\pi$. In this case the light degrees of freedom of the final state are the sum of the light degrees of freedom in the D, plus all of the degrees of freedom in the π, plus the orbital angular momentum between the D and the π; that is, the light degrees of freedom include everything except the heavy quark. In such a decay both J and j_ℓ must be conserved, which leads to new selection rules.

For completeness, a list of other authors who have made predictions about the masses of P-wave charmed mesons includes, [27],[28],[29],[30], [31],[32]. While the earlier papers are sometimes far off the mark, most authors get the splittings close to correct but sometimes have a large shift in the center-of-mass of the multiplet.

3.2 Heavy Flavour Baryons

In this section, the theory of heavy flavour baryons will be discussed in terms of potential models. As for the charmed mesons, other descriptions of these states exist but potential models have been successful and their results can often be presented in closed form. In this section most of the discussion follows that of [17, 33, 34]. In this model the Hamiltonian of a baryon is,

$$H = \sum_{i=1}^{3}(m_i + \frac{p_i^2}{2m_i}) + \sum_{i<j}(H_c^{ij} + H_{BF}^{ij}), \tag{6}$$

where i and j run over the valence quarks inside the baryon. Except for one change, H_c^{ij} and H_{BF}^{ij} are simply the 2-body confining and Breit-Fermi terms from the meson Hamiltonian, equation 2. The exception is that colour factors of 4/3 must be replaced by colour factors of 2/3. This arises from the difference in the strength of the interaction between two quarks compared to that between a quark and an anti-quark. At this point a change of variables is made from the three inter-quark separations to the center-of-mass motion plus two internal coordinates. For the css baryons and the cqq baryons with $q \neq s$, these internal coordinates are defined as,

$$\vec{\rho} = \frac{\vec{r}_1 - \vec{r}_2}{\sqrt{2}} \qquad \vec{\lambda} = \frac{\vec{r}_1 + \vec{r}_2 - 2\vec{r}_c}{\sqrt{6}}. \tag{7}$$

These are illustrated in figure 5. The reduced masses associated with each of these degrees of freedom are,

$$m_\rho = m_q \qquad m_\lambda = \frac{3m_q m_c}{2m_q + m_c}. \tag{8}$$

There is also a conjugate momentum associated with each of these variables. Finally, for the csq baryons the change of variables is a little more complicated and is described in [33].

The quark model also provides a physically intuitive way to build up a picture of the mass spectrum of the Hamiltonian. The one important rule is that the wavefunctions must be antisymmetric under the interchange of identical quarks. Among other things, this will provide a principle which explains the correct order in which to couple the spins of the three quarks.

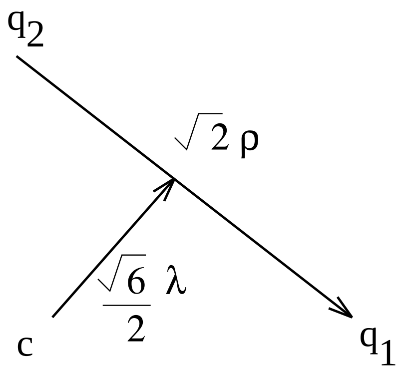

Figure 5: Definition of the ρ and λ variables used in the separation of variables for a charmed baryon, cq_1q_2.

In the quark model, the wavefunctions for the baryons being considered here can be written as simple products of five parts,

$$\psi \quad = \quad \psi_C \, \chi \, \psi_L \, \psi_F \, \psi_R \tag{9}$$

where ψ_C denotes the colour part of the wavefunction, χ denotes the spin wavefunction, ψ_L denotes the angular parts of the spatial wave function, ψ_I denotes the flavour (isospin) wavefunction, and where ψ_R denotes the radial part of the spatial wave function. Each of these pieces will either be symmetric or antisymmetric under the interchange of a pair of quarks. The colour wavefunction is totally antisymmetric under the interchange of a pair of quarks. The ρ angular parts of the spatial wavefunction have an interchange symmetry of $(-1)^{L_\rho}$ under the interchange of quarks 1 and 2, and the λ angular parts of the spatial wavefunction are symmetric under the interchange of quarks 1 and 2. The radial parts of the wavefunction are symmetric under the interchange of quarks. A pair of quarks can either have $S = 0$, which is antisymmetric, or $S = 1$, which is symmetric. The flavour parts will be discussed below. The above breakdown also holds true for the corresponding strange, non-charmed mesons, which will be discussed for purposes of comparison. Not all states in the full theory of all baryons exhibit this factorization and one must worry about cases when, for example, the product $\chi\psi_L$ has a definite interchange symmetry but the individual pieces do not. For the states under consideration in these lectures, however, all of the wavefunctions can be factorized into pieces with definite symmetry.

State	ψ_C	ψ_L	ψ_I	χ
Λ_c	$-$	$+$	$-$	$-\ (S=0)$
Σ_c	$-$	$+$	$+$	$+\ (S=1)$

Table 7: Allowed values of S for the qq diquark inside a the Λ_c or the Σ_c. For example, the negative sign for the Λ_c/ψ_I entry indicates that the isospin part of the diquark wavefunction of the Λ_c is antisymmetric under the interchange of flavour labels.

3.2.1 S-wave Charmed Baryons

The first state to consider is the spatial ground state of the Λ_c, a cud state in which the ud diquark has, by definition, I=0. In the limit that isospin is an exact symmetry, the u and d quarks must be considered identical and the overall wavefunction must be antisymmetric under their interchange. The overall antisymmetry is built up from the pieces of the wavefunction as follows. A ud pair in an $I = 0$ state is antisymmetric under interchange of the flavour indices. The Λ_c is in its spatial ground state so both the ρ and λ degrees of freedom have $L = 0$ and both are symmetric. As always the colour wavefunction is antisymmetric. In order for the overall wavefunction to be antisymmetric under the interchange of the u and d quarks, they must be in a spin 0 state. This is summarized in the first line of table 7. The final step is to combine the spin of the charmed quark with the spin of the diquark. This gives the result that the Λ_c has a total spin[2] of $J = 1/2$. The parity of a baryon in its spatial ground state is positive.

When one applies the same logic to the Σ_c states, which have $I = 1$, one finds that the ud diquark must have $S = 1$. This implies that the spatial ground state of the Σ_c system is a doublet, the members of which have $J^P = 1/2^+$ (Σ_c) and $J^P = 3/2^+$ (Σ_c^*).

In the strange baryon sector, precisely the same logic yields the same general features for the strange, non-charmed baryons, the Λ, Σ and Σ^*. The one important difference is that the splitting of $M(\Sigma_c^*) - M(\Sigma_c)$ should be smaller than the splitting of the $M(\Sigma^*) - M(\Sigma)$. This is a hyperfine splitting which arises from the colour magnetic moment of the c or s quark.

[2] The notation S will be used for the spin of the light diquark while J will be used for the spin of the baryon.

Because $m_s/m_c \simeq 1/3$ in the NRQPM, the splitting is expected to be about 3 times smaller in the charm sector than it is in the strange sector.

The above arguments are summarized in the upper part figure 6. The left hand side shows the measured mass spectrum of the *sqq* baryons, while the right hand side shows that of the *cqq* baryons. The vertical scales on the two sides have different offsets, which have been chosen so that the Λ and Λ_c are at the same level on the page. Otherwise the vertical scale is the same on the two sides. Indeed, the vertical scale is the same, excepting offsets, for all parts of this figure. For both the *sqq* and the *cqq* systems, the spin weighted center-of-mass (*com*) of the Σ states is also shown.

In this figure the smaller hyperfine splitting in the charm sector is evident,

$$\frac{M(\Sigma^*) - M(\Sigma)}{M(\Sigma_c^*) - M(\Sigma_c)} = 2.5 \pm 0.2, \tag{10}$$

which confirms that prediction above is in the right ball park. In order to calculate this ratio some assumptions had to be made about the missing Σ_c^{*+} and Σ_c^{*0}. They were simply ignored, and the mass of the Σ_c^{*++} was used as the center-of-mass of the isospin multiplet. This seems reasonable as the error on the mass of the Σ_c^{*++} is much larger than the expected isospin splitting within the multiplet. Also, the splittings $M(\Sigma_c(com)) - M(\Lambda_c)$ and $M(\Sigma(com)) - M(\Lambda)$ differ by only a small amount, 15 ± 5 MeV. That the difference is small is naturally understood in terms of potential models. When considering the splitting between the Λ and the $\Sigma(com)$, the only thing which contributes is the spin of the light diquark; that is the c or s quark is strictly a spectator. Ultimately this arises from isospin symmetry, which drove the choice of the separation of variables of the Hamiltonian. These observations confirm that it makes sense to talk of these baryons as a diquark, with specific internal properties, interacting with the third quark, s or c. The usual sound-bite is that the quark models are working with "right" degrees of freedom.

Finally, the figure provides a clear answer to a question which often arises when people first encounter charmed baryons. While the decay $\Sigma \to \Lambda\pi$ is forbidden by kinematics, the decay $\Sigma_c \to \Lambda_c\pi$ is allowed. People have asked, "If splittings are supposed to be smaller for heavier mass quarks, why is it not so in this example". The answer is: only the hyperfine splittings involving the c quark are expected to behave as m_s/m_c. The splitting in question, $M(\Sigma) - M(\Lambda)$, is not a hyperfine splitting. Rather it is composed of two pieces, one

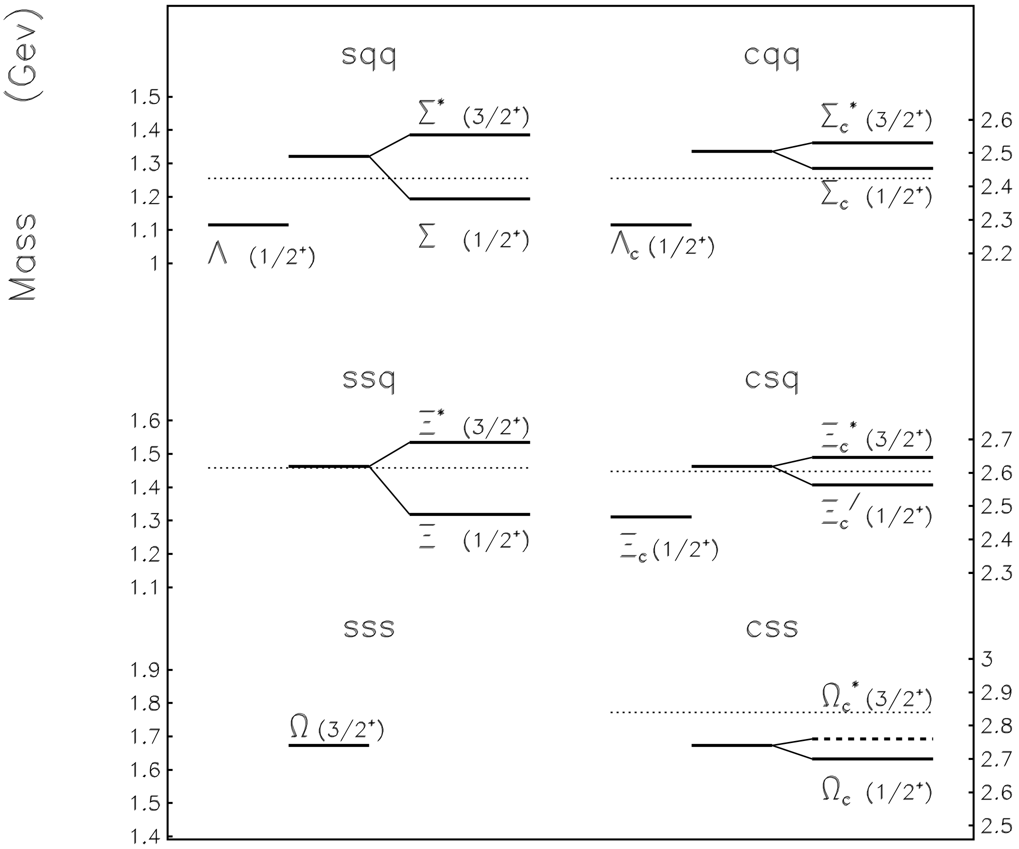

Figure 6: Measured masses of the spatial ground state strange and charmed baryons. The quantities in brackets are the J^P of each state. The unlabeled lines represent the spin weighted center-of-mass of a multiplet. For example, in the upper left part, the unlabeled line is the center-of-mass of the Σ multiplet. In each part of the figure, the dotted line indicates the threshold for decay via π emission to the lowest lying state in that part. In all cases the measurement errors are small compared to the line thickness. The dashed line shows a theoretical prediction for the mass of the unobserved Ω_c^*. The data shown here come from the same sources as that shown in figure 1.

of which is a hyperfine splitting, and which does behave as expected. This same reasoning predicts that the mass splitting $M(\Sigma_b^*) - M(\Sigma_b)$ should be on the order of 25 or 30 MeV and that,

$$M(\Sigma_b(com)) - M(\Lambda_b) \simeq M(\Sigma_c(com)) - M(\Lambda_c). \tag{11}$$

The next sector to consider is the Ξ_c baryons. Because Ξ_c baryons, csu and csd, contain no identical quarks, there is no requirement that the wavefunction be antisymmetric under interchange of any of the constituents. While the identical quark symmetries do not provide an insight into the correct way to couple the three spins, HQET does: because of its small colour magnetic moment, the c quark should be added last. For the same reasons as were discussed in the $Q\overline{q}$ meson section, the total spin, S, of the sq diquark is not a good quantum number. One can, however, start work in a basis of definite S and add perturbations later. When the charmed quark is added to an $S = 0$ diquark it gives the Ξ_c which has $J^P = 1/2^+$. When the charmed quark is added to an $S = 1$ diquark it gives a doublet, the Ξ_c', with $J^P = 1/2^+$, and the Ξ_c^*, with $J^P = 3/2^+$. Finally, in order to find the physical states, the model must allow the two $J^P = 1/2^+$ states to mix. The measured mass spectrum for these states is shown in the right middle section of figure 6. Because of the mixing between the two $J^P = 1/2^+$ states, the center-of-mass of the Ξ^*-Ξ_c' system does not have a simple interpretation but it has been used to set the scale between the left and right halves of the figure.

Because the corresponding strange baryons, ssu and ssd, do contain identical quarks, the antisymmetry rules apply. The ss pair is symmetric under interchange of flavour labels, is in its spatial ground state and has an antisymmetric colour wavefunction. Therefore it must have $S = 1$ and one obtains the familiar baryons, the Ξ with $J^P = 1/2^+$ and the Ξ^* with $J^P = 3/2^+$. This is shown in the left middle section of figure 6. The scales have been set so that the center-of-mass of the Ξ^*-Ξ multiplet is at the same level as the center-of-mass of the Ξ_c^*-Ξ_c' multiplet.

In this figure the smaller hyperfine splitting in the charm sector is again evident. However, because the symmetries of the wave functions are different, there is no simple formula which gives the hyperfine splitting in the charm sector in terms of that in the strange sector.

The last sector in the spatial ground state is the Ω_c sector, css. Here, again, the identical quark symmetries can be used and they require that the

ss pair have $S = 1$. This gives rise to two states, the Ω_c, with $J^P = 1/2^+$, and the Ω_c^*, with $J^P = 3/2^+$. The Ω_c has recently been observed [4] and its mass is plotted in the lower right part of figure 6. The Ω_c^* has not yet been observed and it is indicated by the dashed line in the figure. To compute the position of this line, the predicted Ω_c^*-Ω_c mass splitting was taken from [35] and added to the measured Ω_c mass. It can be seen from this figure that one should expect to see the Ω_c^* only via its decay to $\Omega_c\gamma$, which will be difficult to observe.

The corresponding state in the strange sector is the Ω, sss. This must have a wavefunction which is totally antisymmetric under the interchange of any pair of quarks. Because the flavour and space parts are totally symmetric, and the colour part is totally antisymmetric, the spin part must be totally symmetric. This can only be accomplished if the three quarks have a total spin of 3/2. Thus the Ω has $J^P = 1/2^+$ and its measured mass is drawn in the lower left part of figure 6 at the same level as the center-of-mass of the Ω_c multiplet.

3.2.2 P-wave Λ_c and Σ_c Baryons

Now consider the allowed quantum numbers when one unit of orbital angular momentum is added to a Λ_c or to a Σ_c. This can be added either between the two light quarks or between the light diquark and the charmed quark. Following the nomenclature of the last section, these are known, respectively, as ρ and λ excitations. The mass shift associated with the one unit of angular momentum is given by $\Delta m_\rho = L^2/2m_\rho R_\rho^2$ and $\Delta m_\lambda = L^2/2m_\lambda R_\lambda^2$, where the quantity mR^2 is a moment of inertia. To a first approximation the mean radius of both the ρ and λ excitations should be set by the confinement radius. Therefore the mass splittings should be dominated by the differences in the reduced mass. Because $m_\lambda > m_\rho$, one expects that the λ angular excitations will be the lowest lying spatial excitations of these baryons.

First consider adding one unit of orbital angular momentum to the λ excitation of the Λ_c. Because the ρ excitation is still in an S-wave, the arguments of the previous section imply that the ud diquark must have $S = 0$. This couples with the λ orbital angular momentum to give $j_\ell = 1$. Here the j_ℓ notation defined in the meson sector has been used with the same meaning as before; it is the total angular momentum of everything except the charmed quark. Finally, j_ℓ is split by its hyperfine interaction with the charmed quark to give two states with $J^P = 3/2^-$ and $1/2^-$. This development is shown in the middle of figure 7a). To give an idea of the scale of the mass splittings, the figure also shows the S-wave Λ_c and part b) shows the S-wave Σ_c and Σ_c^*.

When one unit of orbital angular momentum is added to the ρ excitation of the Λ_c, the reasoning of the previous section implies that the ud diquark must have $S = 1$. This couples with the angular momentum to produce $j_\ell = 0, 1, 2$. Each of these is then split by its hyperfine interaction with the charmed quark, to give the five states shown at the top of figure 7a).

When one unit of orbital angular momentum is added to the λ excitation of the Σ_c, the reasoning of the previous section implies that the ud diquark must have $S = 1$. This then couples with the orbital angular momentum to give $j_\ell = 0, 1, 2$. Each of these is then split by its hyperfine interaction with the charmed quark, to give the five states shown in the middle of figure 7b).

Finally, when one unit of orbital angular momentum is added to the ρ excitation of the Σ_c, the reasoning of the previous section implies that the ud diquark must have $S = 0$, which gives $j_\ell = 1$. This is then split by its hyperfine interaction with the charmed quark, to give the doublet shown at the top of figure 7b).

This figure shows that the simple argument that the λ excitations should be at a lower mass than the ρ excitations is borne out in the complete theory, which allows different mean radii associated with each excitation. However the argument only just works in the case of the Σ_c. Notice too that the degeneracy of the ρ and λ excitations switches when one changes from I=0 to I=1.

The lowest lying Λ_c excitations stand well away from the confusion which exists a few hundred MeV above them. Candidates for these states have been observed [5][36][37] at masses of 2592.6 ± 1.3 MeV for the $1/2^-$ state and 2627.3 ± 0.8 for the $3/2^-$ state. These states are believed to be Λ_c excitations, and not Σ_c excitations, because they are observed in the final state $\Lambda_c\pi^+\pi^-$, but not in the final state $\Lambda_c\pi^0$ [5]. The decay $\Lambda_c^* \to \Lambda_c\pi^0$ is forbidden by isospin, but the decay of an excited Σ_c to that same final state is allowed. If the $\Lambda_c\pi^0$ final state were allowed, then phase space requires that, for states so close to the $\Lambda_c\pi\pi$ threshold, the $\Lambda_c\pi$ final state should dominate. Reference [5] also presents a Dalitz plot of the $\Lambda\pi\pi$ final state, a candidate explanation for the relative widths of each state, and a candidate explanation for the absence of a $\Sigma_c\pi$ component in the decay of the higher mass state. Finally, the hyperfine splitting between these two $j_\ell = 1$, P-wave, charmed

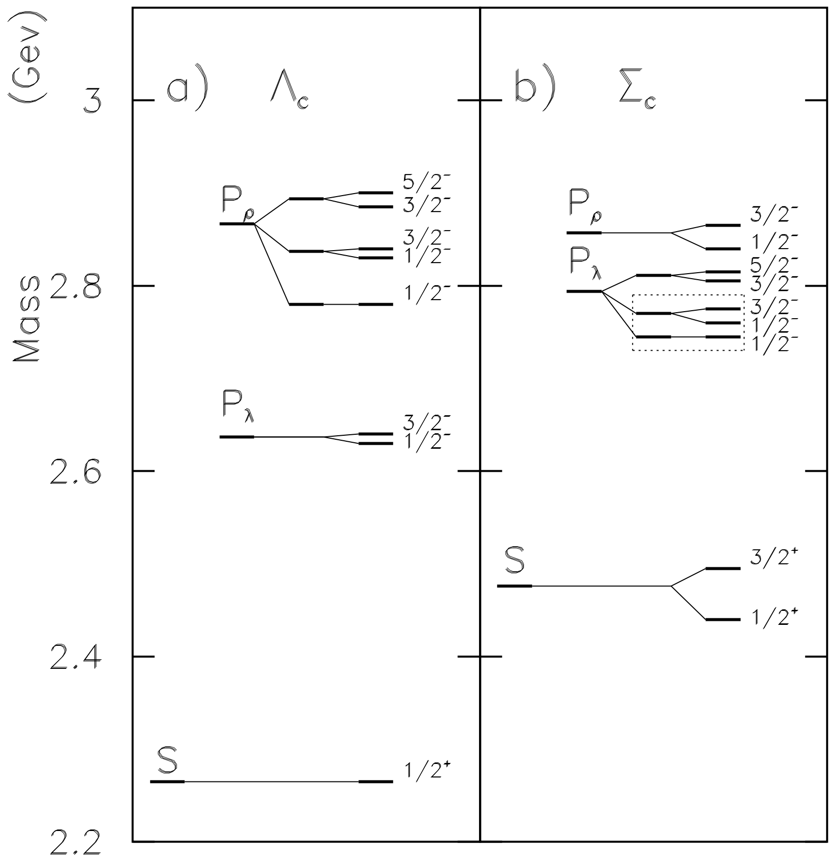

Figure 7: Predicted mass spectrum of S and P wave charmed baryons, from [17]. The region within the dotted lines is drawn with an expanded vertical scale; all of those three states are predicted to lie within about 10 MeV of where the upper one is drawn.

baryon states has been measured to be $34.7 \pm 0.5 \pm 1.2$. This is identical to the splitting observed within the $j_\ell = 3/2$ multiplets of the P-wave charmed and charmed-strange mesons. While one naively expects these splittings to be similar, it appears to be an accident that they are identical.

The relativized quark model [17] overestimates the masses of these two states by about 30 MeV. The model also appears to substantially underestimate the hyperfine splitting, but that may be partly due to the precision with which masses are quoted in their paper. The analogs of these states in the strange sector are the $\Lambda(1520)$ with $J^P = 3/2^-$, and the $\Lambda(1405)$, with $J^P = 1/2^-$. Again one sees the effect of the ratio $m_c/m_s \simeq 3$ on the hyperfine splitting,

$$\frac{M(\Lambda(1520)) - M(\Lambda(1405))}{M(\Lambda_c(2625)) - M(\Lambda_c(2593))} = 3.6 \pm 0.2. \tag{12}$$

3.3 Strong Decays

The favoured model of the strong decays of hadrons is known as the ${}^3P_0$ quark pair creation model (QPCM) and was developed about 1970 by Micu[38] and by Le Yaouanc and collaborators [39, 40, 41]. One of its first successes was to explain the S/D ratio in the decay $b_1(1235) \to \omega\pi$. The basic idea is illustrated by the quark line diagram shown in figure 8. In this model the initial state consists of the $q\overline{q}$ pair, $a\overline{b}$. The strong interaction then creates a new $q\overline{q}$ pair, $c\overline{d}$, from the vacuum and the final state mesons are made by rearranging the four quarks such that the initial constituents, a and $\overline{b}$, end up in different final state mesons. The model is that, relative to the initial state meson, the created pair must have the quantum numbers of the vacuum. That is the created pair must have $IJ^{PC} = 00^{++}$ and there must be no momentum or orbital angular momentum between the two pairs. Consulting table 5 one can see that the only spectroscopic state with $J^{PC} = 0^{++}$ is ${}^3P_0$, hence the name of the model. Moreover the created pair must be in a colour singlet and it must have a flavour wavefunction of $(u\overline{u} + d\overline{d} + s\overline{s})/\sqrt{3}$. That is, there is no explicit flavour dependence but some such dependence may appear via quark mass and phase space effects. The model does not specify the dynamics by which QCD creates the pair. The model has the obvious extension to baryon decay. Finally, the most powerful part of this model is that it has only one free parameter, the overall pair creation strength, which is the same for all strong decays of mesons and baryons.

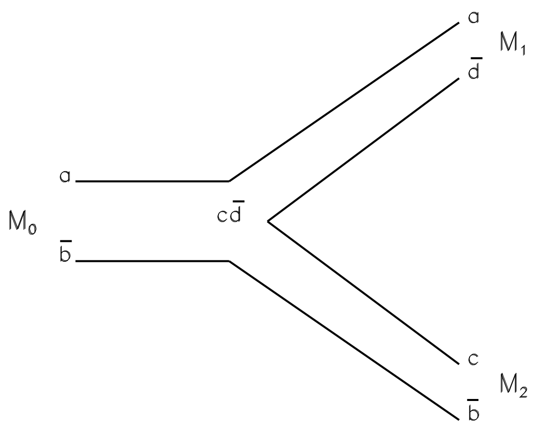

Figure 8: Quark line diagram for the decay of a meson in the $^3P_0$ quark pair creation model.

Within the quark model, one computes transition amplitudes by sandwiching this pair creation amplitude between the initial and final state wavefunctions. What follows, in the general case, is the mother of all angular momentum recoupling problems. However, so long as two or three of the mesons are S-wave mesons, the algebra is reasonable. In this formalism, the partial wave amplitudes for the decay are overlaps of radial wavefunctions and one can covert these to helicity amplitudes using the Jacob Wick identity. An example of the algebra of the full problem, in all of its generality, can be found in [42]. The final answer ends up as a product of four $9j$ symbols.

One aspect of the model which was glossed over above is that it specifies that the created pair creation amplitude is uniform throughout the universe! There have been attempts to modify this by requiring the pair creation to take place inside a flux tube joining the two quarks [43]. However this variation did not produce significantly different results.

3.3.1 Selection Rules

In order to define some notation this section will provide a brief review of angular momentum and parity selection rules. Consider the strong decay $A \to BC$ where the intrinsic parities of the particles are denoted by η_A, η_B, η_C and their intrinsic spins are denoted by J_A, J_B, J_C. To describe the final state in such a decay one also needs to know the allowed values of the orbital angular momentum, L, between the two final state hadrons. In order for the decay to proceed in a partial wave with a given L, that L must satisfy,

$$\vec{J_A} = \vec{L} + \vec{J_B} + \vec{J_C} \tag{13}$$
$$\eta_A = \eta_B \eta_C (-1)^L. \tag{14}$$

Here the symbol L has been used to denote the angular momentum between the final state mesons, not the angular momentum between the quarks in one of the mesons. It should be clear from the context which is meant in any future part of the discussion — in one case a phrase "P-wave mesons" will be used and in the other case a phrase like "D-wave decays" or "S-wave transitions" will be used.

Consider, for example, the decays of the P-wave D mesons. Start by looking at figure 8 with an initial state of $c\overline{q}$, where $q = u, d$. Now, consider what sort of final states can be made by the various combinations of quarks: $D\pi$, $D^*\pi$, D_sK, D^*_sK, $D\eta$, D_ρ, D_sK^*, $D(\pi\pi)_{\mathrm{non-res}}$ and so on. Next, remember that these states are found about 500 MeV above the center-of-mass of the S-wave multiplet. Therefore, the only decays which are certain to be important are $D\pi$ and $D^*\pi$. Most other modes are either kinematically forbidden or are strongly suppressed by phase space. Some authors [44], however, have suggested that the decay $D\rho$ may contribute significantly via the low mass tail of the ρ. It has also been suggested the non-resonant $\pi\pi$ transitions may be found; however there are few examples in particle physics in which a non-resonant $\pi\pi$ transition competes favourably with a fully allowed resonant transition, such as $D\pi$ or $D^*\pi$. The decays to $D\pi$ and $D^*\pi$ decays are well established but there are no experimental limits on the presence of $D\rho$, $D^*\rho$ or non-resonant $D\pi\pi$. Finally, table 8 shows, for each of the established decays, the partial waves which are allowed by the selection rules 13 and 14.

The same exercise for the P-wave charmed-strange mesons leads to the conclusion that the allowed final states are DK and D^*K. The K^* is certainly too narrow to contribute any significant rate through its low mass tail. The experimentally established decays are indeed to DK and D^*K. Notice that the final state $D_s\pi^0$ is both OZI forbidden and isospin forbidden, while the final state $D_s\pi\pi$ is OZI forbidden.

Decay	Allowed Partial Waves
$D_2^* \to D\pi$	D
$D_2^* \to D^*\pi$	D
$D_1 \to D\pi$	forbidden
$D_1 \to D^*\pi$	S, D
$D_0^* \to D\pi$	S
$D_0^* \to D^*\pi$	forbidden

Table 8: Allowed partial waves for decays of P-wave $c\overline{q}$ mesons. No HQET selection rules have been applied.

3.3.2 Partial Widths

Shortly after the first P-wave charmed meson was discovered, Rosner [18] published a model of the level structure the P-wave charm system. This model also made estimates for the partial widths of the decays listed in table 8. That derivation will be sketched below. He first wrote down the states in the ${}^3P_1 - {}^1P_1$ basis, and computed the mass matrix, which has the following non-diagonal part,

$$M \begin{bmatrix} {}^3P_1 \\ \\ {}^1P_1 \end{bmatrix} = \begin{bmatrix} \overline{M} + \frac{1}{2}(c_T - c_1 - c_2) & \frac{1}{\sqrt{2}}(c_2 - c_1) \\ \\ \frac{1}{\sqrt{2}}(c_2 - c_1) & \overline{M} - \frac{3}{4}c_H \end{bmatrix} \begin{bmatrix} {}^3P_1 \\ \\ {}^1P_1 \end{bmatrix}. \tag{15}$$

Here $\overline{M}$ is the center-of-mass of the multiplet and the various c coefficients are defined by equation 3. The eigenstates of this mass matrix are found by mixing the two $J^P = 1^+$ states into the combination which diagonalizes the mass matrix,

$$\begin{aligned} |\alpha> &= \cos\phi|{}^3P_1> + \sin\phi|{}^1P_1> \\ |\beta> &= -\sin\phi|{}^3P_1> + \cos\phi|{}^1P_1>, \end{aligned} \tag{16}$$

where the mixing angle, ϕ, is specified by,

$$\tan\phi = \frac{c_1 - c_2}{\sqrt{2}(\overline{M} - M_\alpha)} = \frac{\sqrt{2}(M_\beta - \overline{M})}{c_1 - c_2}. \tag{17}$$

In the limit that $m_c \to \infty$ the mixing angle becomes ϕ_0, which is given by $\tan\phi_0 = 1/\sqrt{2}$. Finally, the reduced partial widths of each state, $\tilde{\Gamma}$, are given by,

$$
\begin{aligned}
\tilde{\Gamma}(D_2^* \to D^*\pi) &= \frac{3}{10}D^2 \\
\tilde{\Gamma}(D_2^* \to D\pi) &= \frac{1}{5}D^2 \\
\tilde{\Gamma}(D_1(\alpha) \to D^*\pi) &= \frac{1}{2}\left(S^2\cos^2(\phi-\phi_0) + D^2\sin^2(\phi-\phi_0)\right) \\
\tilde{\Gamma}(D_1(\beta) \to D^*\pi) &= \frac{1}{2}\left(S^2\sin^2(\phi-\phi_0) + D^2\cos^2(\phi-\phi_0)\right) \\
\tilde{\Gamma}(D_0^* \to D\pi) &= \frac{1}{2}S^2.
\end{aligned} \tag{18}
$$

Here a "reduced" width means the phase space factors have been set equal for all states. The quantities S and D are partial wave amplitudes which, in the quark model, are just overlaps of radial wave functions. In potential models all of the P-wave charmed mesons have the same radial wave function and all of the S-wave charmed mesons have the same radial wavefunction. Therefore D is just a single number which is the same wherever it appears in equation 18; it is not an expression which takes on different values for different decays. Similarly for S. In this model, indeed in all models, the width of the D_2^* is on the order of 20 MeV and the width of the D_0^* is on the order of 100 to 400 MeV. Therefore, predictions for the widths of the two D_1 states are sensitive to the predicted mixing angle.

In the limit that $m_c \to \infty$, these partial widths exhibit two interesting properties. First, the $D_1(\alpha)$ state decays in a pure S-wave while the $D_1(\beta)$ state decays in a pure D-wave. Second, the reduced total width of the D_2^* is equal to that of the $D_1(\beta)$ state and the reduced total width of the D_0^* is the same as that of the $D_1(\alpha)$ state. In physics zeros and ones are rarely accidents but, instead, are usually the results of symmetries. In this case, the above observations are the result of Heavy Quark Symmetry (HQS). Now the question arises, can one use HQS to get the results directly, without the need for the intermediate machinery of a potential model?

3.3.3 HQET Selection Rules

In the limit $m_c \to \infty$, one considers the four P-wave charmed mesons to be only two distinct states, with one with $j_\ell^P = 1/2^+$ and one with $3/2^+$.

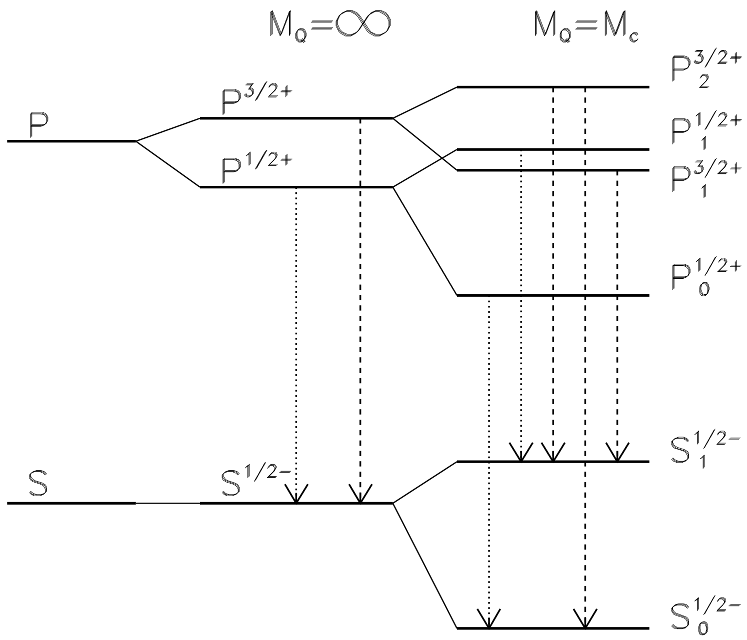

Figure 9: HQET Selection rules for the decay of P-wave charmed mesons. The S-wave transitions are indicated by dotted lines and the D-wave transitions are indicated by dashed lines. This figure is not to scale.

Similarly the two S-wave charmed mesons are considered to be a single state with $j_\ell^P = 1/2^-$. So there are only two independent transitions, $P^{3/2^+} \rightarrow S^{1/2-}\pi$ and $P^{1/2^+} \rightarrow S^{1/2+}\pi$[45]. The first of these has the j_ℓ^P structure, $3/2^+ \rightarrow 1/2^-\ 0^-$, which can only proceed in a D-wave. Similarly, the second decay has the j_ℓ^P structure $1/2^+ \rightarrow 1/2^-\ 0^-$, which can only proceed in an S-wave. These rules hold true for each $P_J^{j_\ell P}$ component of each $P^{j_\ell P}$ state, not just for the overall multiplet. For example, $P_1^{3/2+} \rightarrow D^*\pi$ may only proceed in a D-wave. This picture also explains why the total width of the $P_2^{3/2+}$ is the same as that of the $P_1^{3/2+}$ — because, in the $m_c \rightarrow \infty$ limit they are identical states.

The above discussion is illustrated in figure 9. The left hand part of that figure shows the centers of mass of the S-wave and P-wave multiplets. The middle section shows the mass spectrum and transitions in the $m_c \rightarrow \infty$ limit; the dotted line shows the S-wave transition and the dashed line shows the D-wave transition. The right hand part of the figure shows the spectrum and transitions when the heavy quark has the mass of the charmed quark. In that case, the rules derived above remain approximately true (although the figure shows them as exactly true). The rules will not be exactly true because the two $J^P = 1^+$ states will mix with each other. To summarize, this short discussion has reproduced, without any mathematics, the results obtained in the previous section. One can use this to identify Rosner's α state as the $P_1^{1/2+}$ and his β state as the $P_1^{3/2+}$.

One of the questions also addressed by this formalism is how to predict the ratio, $\Gamma(D_2^* \to D\pi)/\Gamma(D_2^* \to D^*\pi)$. Both of these branching fractions are proportional to some symmetry coefficient, which may only depend on the angular momenta in the problem, multiplied by a common overall strength. So predicting the ratio reduces to calculating the symmetry coefficients. The most straightforward discussion of this can be found in [46], which identifies the symmetry coefficient as nothing more than a $6-j$ symbol.

However HQET itself does not predict one important thing — the size of the violation of the strict HQET limit. For example, in the HQET limit $\Gamma(P_1^{1/2+})$ is on the order of 100 to 400 MeV, while $\Gamma(P_1^{3/2+})$ is on the order of 20 MeV. So even a small violation of the HQS limit may cause enough mixing between the 1^+ states to make a profound difference in the observed decay patterns. Using only HQET, one can make only a limited statement about the S-wave partial width of the $P_1^{3/2+}$: it is small compared with typical S-wave partial widths, such as $a_1 \to \rho\pi$. It says nothing about the relationship between the S-wave and D-wave partial widths. Nevertheless the following misconception about HQET is often repeated: in the decay $P_1^{3/2+} \to D^*\pi$, HQET predicts that the D-wave amplitude will dominate over the S-wave amplitude. While all models do indeed predict this, HQET itself does not. At first glance, the data appears to confirm this prediction, but, as will be discussed in section 5.3, the data actually provides a surprisingly poor constraint on the amount of S-wave allowed in this decay.

In order to make predictions of the amount of 1^+ mixing, and therefore of the amount of S-wave in the decay of the $P_1^{3/2+}$, one must resort to models. At present the only model to include this effect is that of Godfrey and Kokoski [20]. Their predictions for the D and D_s sectors can be found in table 9. Their model does indeed predict that the $P^{3/2+}$ will decay mostly via a D wave. However something interesting happens in the D_{s1}: because the decay is so close to threshold, the p^5 phase space factor heavily suppresses the

Decay	Partial	Γ(MeV)			
	Wave	Ref [20]a	Ref [20]b	Ref [20]c	Ref [44]
$D_2^* \to D^* \pi$	D	19	17	14	9
$D_2^* \to D \pi$	D	44	35	23	16
$D_2^* \to D^* \rho$					3
$D_1(j_\ell = 1/2) \to D^* \pi$	S	250	270	1100	
	D	0.53	0.48	0.34	
$D_1(j_\ell = 3/2) \to D^* \pi$	S	6.0	6.7	26	0
	D	20	17	12	11
$D_1(j_\ell = 3/2) \to D \rho$	D				6
$D_0^* \to D \pi$	S	290	170	990	
$D_{s2}^* \to D^* K$	D	1.0	1.4	1.0	< 1
$D_{s2}^* \to D K$	D	20	26	15	7
$D_{s1}(j_\ell = 1/2) \to D^* K$	S	140	300	860	
	D	$\simeq 0$	$\simeq 0$	$\simeq 0$	
$D_{s1}(j_\ell = 3/2) \to D^* K$	S	0.31	0.64	1.82	
	D	0.05	0.07	0.04	< 1
$D_{s0}^* \to D K$	S	310	270	990	

Table 9: Predicted decay rates for strong decays of P-wave charmed mesons, in MeV. The results from [20] are for a) their pseudoscalar emission model, b) their equal radii model and c) their effective radii model.

D-wave amplitude. It is so strongly suppressed that the HQET suppressed S-wave amplitude dominates. This conclusion is also reached by another group [47]. They do not calculate the amount of mixing but instead show that for a reasonable range of assumptions about the mixing angle, the S-wave decay dominates. Again, the data does not provide a strong constraint on the relative amounts of D-wave and S-wave.

The final picture of the charmed and charmed-strange P-wave mesons is quite simple. There should be six states with $j_\ell^P = 3/2^+$, which have widths on the order of 1 to 20 MeV, and six states with $j_\ell^P = 1/2^+$, which have widths on the order of 100 to 400 MeV. All six $3/2^+$ states have been observed.

3.4 Electromagnetic Decays

Both of the decays $D_s^* \to D_s\gamma$ and $D^* \to D\gamma$ are magnetic dipole (M1) decays, which proceed by one quark flipping its spin and emitting a photon. The matrix element is a coherent sum over the spin flip amplitudes for the two quarks [10],

$$A(D^* \to D\gamma) \quad \propto \quad \langle D|\,(\mu_Q\vec{\sigma}_Q + \mu_{\overline{q}}\vec{\sigma}_{\overline{q}}) \cdot \vec{\epsilon}|D^*\rangle\,. \tag{19}$$

Here $\vec{\epsilon}$ is the polarization vector of the emitted photon, quantized along the quantization axis of the initial D^*; that is, it is not the helicity of the photon. Also, $\vec{\sigma}_i$ is a Pauli matrix which operates on the spins of constituent i, and $\mu_i \propto e_i/m_i$ is the magnetic moment of the constituent. In a potential model the wave functions of the D and D^* are identical except for their spin parts and the above amplitude can be computed using the identity,

$$\vec{\sigma} \cdot \vec{\epsilon} \quad = \quad -\frac{1}{2}(\sigma_+\epsilon_- + \sigma_-\epsilon_+) + \sigma_z\epsilon_z, \tag{20}$$

where $\sigma_\pm = \mp(\sigma_x \pm i\sigma_y)$ are the spin raising and lowering operators. For example, when the D^* is in a state with a magnetic quantum number of $+1$, its spin wavefunction is $|\uparrow\uparrow\rangle$, where the order is $|Q\overline{q}\rangle$. The spin wavefunction of the D meson is $\left|(\uparrow\downarrow - \downarrow\uparrow)/\sqrt{2}\right\rangle$. For a D^* in this state, only the σ_- parts of the amplitude are non-zero, and the decay rate is,

$$\Gamma(D^* \to D\gamma) \quad \propto \quad \left|\left\langle \frac{1}{\sqrt{2}}(\uparrow\downarrow - \downarrow\uparrow)\,|(\mu_Q\sigma_{Q-} + \mu_{\overline{q}}\sigma_{\overline{q}-})|\uparrow\uparrow\right\rangle\right|^2$$

$$\begin{aligned} &\propto \quad \left|(-\mu_Q + \mu_{\overline{q}})\right|^2 \qquad (21)\\ &\propto \quad \left|(\mu_Q + \mu_q)\right|^2 . \end{aligned}$$

This last form is the usual way in which the transition amplitude is reported, which can be a little misleading since it is expressed in terms of the charge of q, not in terms of the charge of the $\overline{q}$. The other components of the σ operators describe the transition for the other magnetic substates of the D^* and they lead to the same final expression.

This exercise can be summarized as follows. For the radiative decays of the D^{*+} and D_s^{*+}, there is destructive interference between the amplitudes for photon emission from the two quarks. On the other hand, for the radiative decay of the D^{*0} the interference is constructive. Using typical potential model values of $m_u = m_d = 300$ MeV and $m_c = 1500$ MeV leads to,

$$R_\gamma^{+0} = \frac{\Gamma(D^{*+} \to D^+\gamma)}{\Gamma(D^{*0} \to D^0\gamma)} \quad \simeq \quad 0.05. \qquad (22)$$

Because of angular momentum and parity conservation, the photon must be emitted in a P-wave. Therefore the correction for differences in phase space multiplies the above ratio by a factor of $(p_+/p_0)^3$. Here p_+ is the momentum of the photon, in the rest frame of the D^{*+}. Similarly for p_0. This correction amounts to only a few percent.

The history of the measurements of the D^* branching fractions is summarized in figure 10. In each section, the upper data points show the early measurements of the various branching fractions. The average of these points, as reported by the Particle Data Group in 1992 [48], is shown next. The diamonds without error bars show the results of a typical theoretical calculation [18]. The agreement between the 1992 world average values and the theory is poor and the biggest problem lies in the value of $B(D^{*+} \to D^+\gamma)$.

The essence of the disagreement can be seen as follows. Consider the two ratios,

$$R_\gamma^0 \quad = \quad \frac{B(D^{*0} \to D^0\gamma)}{B(D^{*0} \to D^0\pi^0)} \qquad (23)$$

$$R_\gamma^+ \quad = \quad \frac{B(D^{*+} \to D^+\gamma)}{B(D^{*+} \to D^+\pi^0)}. \qquad (24)$$

One can measure these two ratios and then relate the denominators using isospin and a correction for differences in phase space. This allows one to

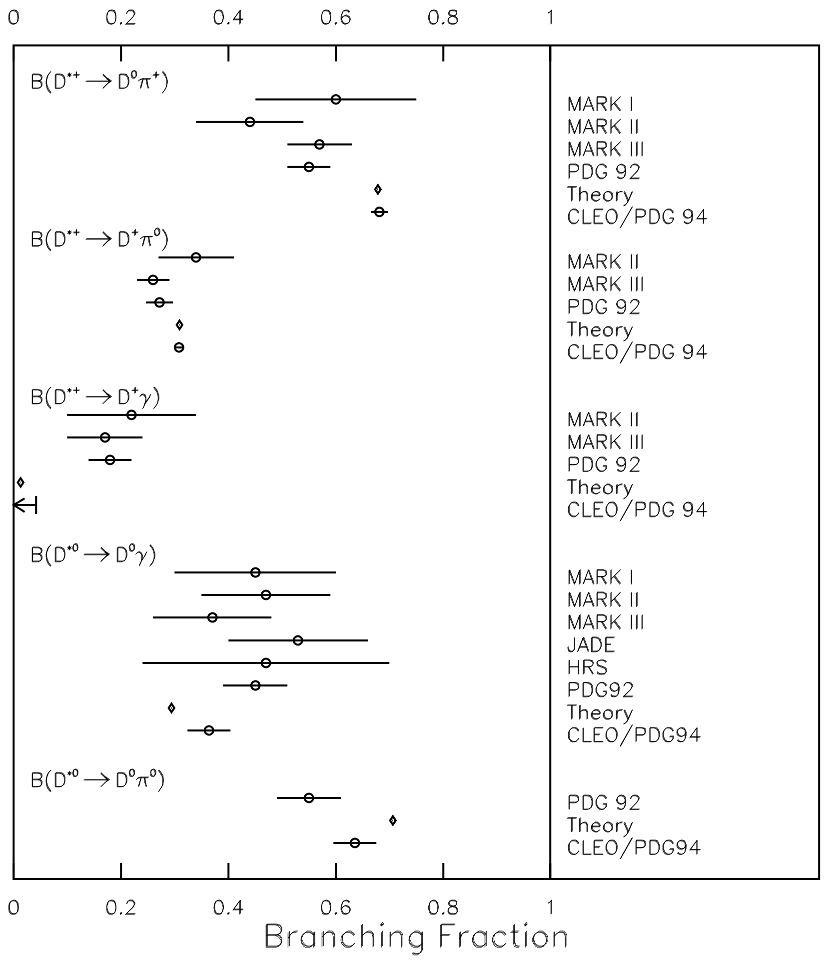

Figure 10: History of Measurements of the D^* branching fractions.

extract a value for R_γ^{+0} which is in disagreement with equation 22. If the 1992 data were correct then, either equation 22 is horribly wrong or the phase space correction is horribly wrong. No one believed that either of these calculations was seriously wrong and, for many years, there was a question mark hanging over the data.

In 1992 the question was resolved in favour of the theory by new CLEO measurements[8] of R_γ^0 and R_γ^+. These measurements are shown as the final data points in each section of figure 10. One might argue that the D^{*+} points agree with the theory too well, and, in fact, they do. The measurement made by CLEO was only of the two ratios R_γ^0 and R_γ^+. In order to turn these into the data points shown in the figure, three constraints were needed,

$$B(D^{*+} \to D^+\pi^0) + B(D^{*+} \to D^0\pi^+) + B(D^{*+} \to D^+\gamma) = 1 \tag{25}$$

$$B(D^{*0} \to D^0\pi^0) + B(D^{*0} \to D^0\gamma) = 1 \tag{26}$$

$$\frac{B(D^{*+} \to D^0\pi^+)}{B(D^{*+} \to D^+\pi^0)} = 2.21 \pm 0.07 \tag{27}$$

The last constraint is the consequence of isospin symmetry corrected for the differences in phase space. Its small error was made possible by improved measurements of the $D^* - D$ mass splittings [49]. Because this same constraint is also built into any theory, if $B(D^{*+} \to D^+\gamma)$ is small, then the experiment can only reproduce the theoretical predictions for the other two D^{*+} modes.

The above results are not correctly reported in the 1994 Review of Particle Properties [6]. The Particle Data Group decided that the CLEO results were of sufficient quality that it no longer included the previous results in their overall fit. Their fitting procedure includes the constraints in equations 25 and 26. When they fed the CLEO branching fractions into their fit, these two constraints were applied a second time. This incorrectly reduced the errors quoted in the Review of Particle Properties. The central values are correctly reported. The correct errors are given in table 4.

3.5 $D_s^* \to D_s\pi^0$ and Isospin Conservation

The strong decay $D_s^* \to D_s\pi^0$ provides an opportunity to see how isospin conservation works at the quark level. Figure 11 a) shows one quark line diagram through which the decay $D_s^* \to D_s\pi^0$ can proceed. While this

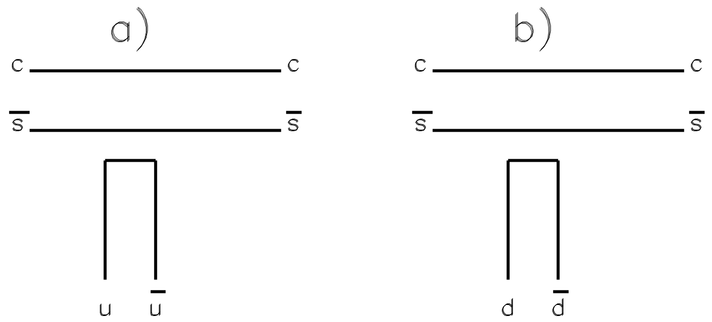

Figure 11: Isospin conservation, at the quark level, in the decay $D_s^* \to D_s\pi^0$.

diagram is OZI suppressed it is not identically zero and one can imagine that it might compete with a radiative decay. However there is a second diagram, shown in Figure 11 b) which can also contribute to the decay. Because the strong interactions do not see any difference between the u and d quarks, the two diagrams in Figure 11 have identical amplitudes. They will constructively interfere for final states of the form $D_s(u\overline{u}+d\overline{d})$, such as $D_s\eta$, but they will destructively interfere for final states of the form $D_s(u\overline{u}-d\overline{d})$, such as $D_s\pi^0$. In the limit that isospin is an exact symmetry this cancelation is exact.

Cho and Wise [50] recently proposed a mechanism through which the decay $D_s^* \to D_s\pi^0$ might proceed. In their model, the D_s^* decay proceeds via a virtual η which mixes into a π^0 via an isospin violating strong interaction proportional to $(m_u - m_d)(m_s - (m_u + m_d)/2)$. The decay to the virtual η occurs through the $s\overline{s}$ component of the η and so it is an OZI allowed decay. They note that the D_s is a likely place to observe such a small effect because its total width is small. Not only is its dominant decay an electromagnetic one, but even that decay is suppressed by the partial cancelation of the magnetic moments of the two quarks. Recently CLEO has presented evidence for this decay [1] and obtain,

$$\frac{\Gamma(D_s^* \to D_s\pi^0)}{\Gamma(D_s^* \to D_s\gamma)} = 0.062^{+0.020}_{-0.018} \pm 0.022. \tag{28}$$

Because the Q value of this decay is small, the resolution on the mass difference $M(D_s^*) - M(D_s)$ is also small, and the mass difference can be precisely measured, even with a small number of events. The 15 events observed in this mode contribute a precision about equal to that of several hundred events in the final state $D_s\gamma$. The 1994 Particle Data Group value for this mass difference was 141.6 ± 1.8 MeV. Since then CLEO has published a value of $144.22 \pm 0.47 \pm 0.37$ MeV using $D_s\gamma$ and a value of $143.76 \pm 0.39 \pm 0.40$ MeV using $D_s\pi^0$. Because these measurements are independent they can be averaged, which gives a mass difference of 143.97 ± 0.41.

The observation of this new decay mode provides the first significant constraints on the J^P of the D_s^*. A state which decays by a parity conserving interaction into two pseudoscalars must have natural J^P. Because the D_s^* also decays to $D_s\gamma$ it cannot have a spin of zero. This leaves the possibilities, $1^-, 2^+, 3^- \ldots$, which includes the quark model expectation of 1^-.

4 Survey of Experimental Techniques

While a great variety of experiments have contributed to the study of the ground state D^+ and D^0 mesons, most of the results in the spectroscopy and decays of the heavier charmed states has come from five experiments, ARGUS, CLEO, Fermilab experiments E691 and E687, and from CERN WA89. These five experiments form three distinct classes.

One class includes ARGUS [51] and CLEO [52], universal 4π magnetic spectrometers, which operate at e^+e^- rings with a center-of-mass energy of about 10 GeV. ARGUS is located at the DORIS II storage ring at DESY and took data for about 10 years, starting in 1982. The collaboration is still producing physics results with this data set. CLEO, which has now operated for more than 10 years, is located at CESR at Cornell University. The detector is continuing to take data and, with an approved upgrade program, will do so well into the future. One advantage enjoyed by these experiments is that the charm production cross-section is approximately 40% of the total hadronic cross-section. Moreover, because the beam energy is relatively low, the multiplicity of charm events is also reasonably low. Typically only a few additional pions accompany each charmed hadron. Historically the two detectors competed on a reasonably equal footing, with the edge in luminosity going to CLEO and the edge in detector quality going to ARGUS. However, the CLEO detector has continued to evolve while the ARGUS data taking has come to an end. The main differences between ARGUS and the present version of CLEO are the magnetic field of the analyzing magnet, the electromagnetic calorimetry, and the luminosity delivered by the storage ring.

CLEO runs with a magnetic field of 1.5 T compared with 0.8 T for ARGUS. Therefore CLEO has better momentum resolution at the cost of less efficiency at low p_T. The ARGUS calorimetry is a lead-scintillator sandwich design and was a major advance in its time; in particular, it was placed inside the coil of the analyzing magnet. In the late 1980's CLEO upgraded their calorimetry to CsI crystals, also placed inside the analyzing magnet. This crystal calorimeter obtains energy resolutions about 4 times better than does ARGUS. Indeed this calorimeter is unique among the magnetic spectrometer experiments contributing the study of heavy flavour spectroscopy. Finally, the biggest advantage enjoyed by CLEO, over all of its competitors, is that the CESR storage ring continues to set world records for both instantaneous luminosity and for integrated luminosity delivered over a year.

The second class of experiments includes FNAL experiments E691 and E687, which use a high energy photon beam striking a fixed Be target. Both of these experiments have finished data taking and E687 is still producing results. The advantage that these experiments enjoy is a larger production cross-section for charm. However this cross-section is only a tiny part of the total hadronic cross-section, which complicates triggering, data acquisition, and data reduction. On the other hand, the background level is still much lower than is found in hadron beam fixed target experiments. Therefore, using a high energy photon beam is an excellent operating point in the space of signal cross-section and background level. The tool which makes these experiments work is their silicon microstrip vertex detectors (SMD). For example, in the E691 apparatus, the mean decay lengths of D^+ and D^0 mesons are, respectively, 8.5 mm and 3.3 mm. For comparison, the resolution on the decay length is typically 0.440 mm. Because most of the backgrounds have a decay length of zero, this provides a powerful tool to reject random combinations of tracks which happen to lie in the mass region of interest. Historically, the inclusive D^0 and D^+ yields from these detectors have been comparable to those from the e^+e- machines. However, because of their SMDs, the fixed target experiments have a much better signal to background ratio for those D^0 and D^+ modes in which all of the daughters are charged.

The final class of experiments includes just CERN WA89 which uses a Σ^- beam incident on a fixed target. The goal of this experiment is to investigate hadron production mechanisms in which the charmed particle shares a spectator quark with the beam particle. It is hoped that these processes will lead to an enhancement in the production rate of charmed baryons, in particular that of charmed-strange baryons. This experiment also relies heavily on its silicon microstrip vertex detectors. Another important feature of the detector is its RICH system used for particle identification.

Many other groups have contributed to heavy flavour spectroscopy but their contributions have, in these lectures, been buried in the references to the Review of Particle Properties. For example, the LEP experiments and CDF have contributed the measurement of the mass of the B_s. The only measurement of any Σ_c^* state comes from a Serpukov heavy liquid bubble chamber group. An ITEP bubble chamber group has made contributions to the study of D_s mesons and their excited states. The CUSB group made observations of the B^*. Other groups have made contributions which have since been superseded. The Mark I, II and III groups made important early contributions to the study of D^* mesons and numerous fixed target experiments provided measurements of the weakly decaying charmed baryons.

4.1 Continuum Charm Production in e^+e^- Machines

The main physics interest of the ARGUS and CLEO collaborations is the study of the decays of B mesons and, therefore, their e^+e^- colliders usually operate at the energy of the $\Upsilon(4S)$ resonance. Figure 12 shows the measured total hadronic cross-section in the energy range that CLEO operates. Notice the broken horizontal scale. The three narrow structures, at energies of about 9.46, 10.02 and 10.35 GeV, are, respectively, the $\Upsilon(1S)$, $\Upsilon(2S)$ and $\Upsilon(3S)$ resonances. These are understood to be $b\overline{b}$ bound states which are kinematically forbidden to decay into two B mesons. Their dominant decay mode is via OZI suppressed strong decays, which explains their narrow width. There is no significant charm production from these resonances. The figure also shows the threshold for $B\overline{B}$ production and the low, broad resonance immediately above this is the $\Upsilon(4S)$. This is also understood as a $b\overline{b}$ bound state and its greater width is explained by the $B\overline{B}$ final state being kinematically allowed. Indeed the $\Upsilon(4S)$ is believed to decay almost 100% of the time to $B\overline{B}$.

The baseline level of the cross-section in figure 12 comes from the reaction, $e^+e^- \to q\overline{q}$, where $q = u, d, s, c$, followed by the hadronization of the $q\overline{q}$ pair. About 40% of the time the initial $q\overline{q}$ pair is a $c\overline{c}$ pair. The hadronization process typically produces two collimated jets of hadrons but it cannot create any new charmed quarks [53]. Therefore all charmed hadrons produced

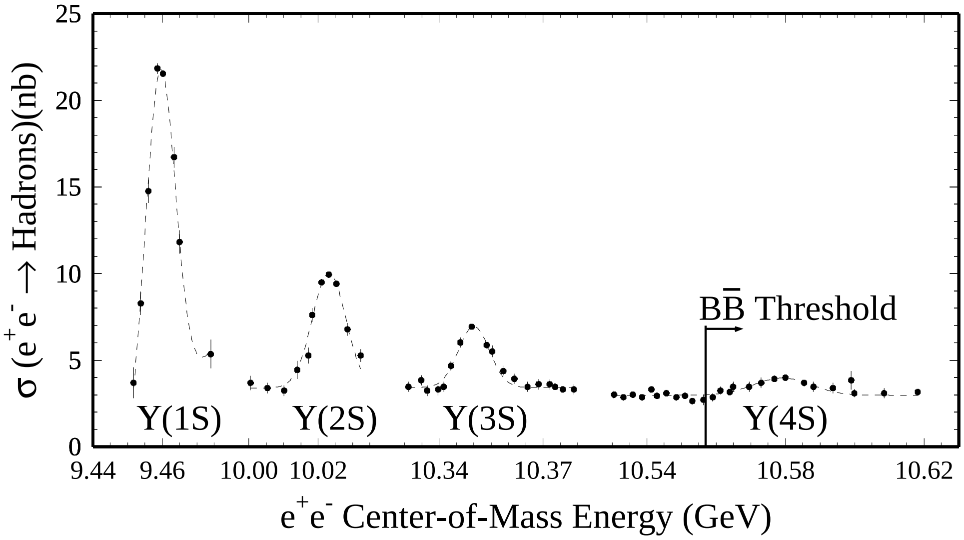

Figure 12: Visible hadronic cross section as a function of center-of-mass energy for e^+e^- collisions in the neighbourhood of the Υ resonances. Notice the gaps in the horizontal scale.

by this mechanism contain one of the initial $q\overline{q}$ pair. Charmed hadrons produced in this fashion are said to come from "continuum production". One of the properties of continuum production is a pronounced leading particle effect: a final state hadron which contains one of the primary $q\overline{q}$ has a much higher average momentum than other particles produced in the hadronization process. The jargon used in these experiments is that the hadronization processes is known as fragmentation, the momentum spectrum is known as the fragmentation function, and the leading particle effect is called "having a hard fragmentation function". Moreover the excited charm states tend to have a harder fragmentation function than do the ground states. Usually one discusses fragmentation functions in terms of the scaled momentum, $x_p = p/\sqrt{E_{beam}^2 - m^2}$, where p and m are the momentum and mass of the candidate and where E_{beam} is the beam energy. If one requires that $x_p > 0.5$, one will accept between about 60% and 85% of the charmed particles and will reduce the combinatoric background by a factor of at least 15 to 20.

There is a second, copious source of charmed hadrons in the events collected by CLEO and ARGUS. When a b quark decays, about 99% of the time it produces a c quark and a W boson. Understanding the remaining rare decay modes is one of the main challenges facing both CLEO today and B-factories in the future. A charmed quark produced via $b \to cW$ will hadronize as a charmed hadron and, perhaps, some additional light hadrons. Most of the time the W has sufficient mass to decay into either a $u\overline{d}$ or a $c\overline{s}$ pair but phase space considerations ensure that it usually decays into a $u\overline{d}$ pair. The net result is that for every B meson decay, about 1.15 charmed hadrons are produced. The precise value of this number is currently the subject of a great deal of experimental and theoretical effort. However the momentum spectrum of charmed particles from B decay is soft; the kinematics of the two step decay chain, ensures that they must have $x_p < 0.5$. Therefore, this source of charm has a poor signal to background ratio and is usually not used in studies of charm spectroscopy at ARGUS and CLEO.

4.2 The D^* Trick

One of the important tools available to people working in charm spectroscopy is the so called "D^* trick", which exploits the small Q value in the decays $D^* \to D\pi$. A list of Q values for the three different decays is given in table 4. The first consequence of the small Q value is that there is little phase space available for combinatoric background. A second consequence is that the resolution on the mass difference $\Delta m = M(D\pi) - M(D)$ is narrow. In the CLEO detector, for example, the resolution is less than 1 MeV (σ) for a broad range of D^* momenta. The combination of these two properties ensures that D^* signals have an excellent signal to background ratio. This, in turn, results in relatively good signal to background ratios for objects which decay into D^* mesons. This trick is especially important at the e^+e^- machines which have much poorer D signals than do the fixed target experiments.

While a proper explanation of the excellent resolution on Δm is beyond the scope of these lectures, a few parts of the story stand on their own. The bottom line is that, when measuring Δm, one is measuring the Q value and adding it to the mass of the pion. Therefore, even a 20% error on the Q value results in a resolution on Δm on the order of 1 MeV. Another piece of the puzzle is to see that most of the errors contributing to the error on the D^* mass also contribute to the error on the D mass. These errors largely cancel in Δm.

The following, somewhat simplistic, picture might also shed some light on the subject. First, one can then write,

$$\begin{aligned}\Delta m &= \frac{m_{D\pi}^2 - m_D^2}{m_{D\pi} + m_D} &(29)\\ &= \frac{m_\pi^2 + 2E_D E_\pi - 2p_D p_\pi \cos\theta}{m_{D\pi} + m_D}, &(30)\end{aligned}$$

where θ is the opening angle between the D and the π. For a D^* with momentum above, say, 1 GeV, one can make the approximation that the Q value is zero, everywhere except in the $\cos\theta$ term. In this case, the Lorentz boost equations from the D^* frame to the lab frame are,

$$E_D = \gamma m_D, \quad p_D = \beta\gamma m_D, \quad E_\pi = \gamma m_\pi, \quad p_\pi = \beta\gamma m_\pi, \tag{31}$$

where $\beta = p_{D^*}/E_{D^*}$, $\gamma = E_{D^*}/M_{D^*}$, and where everything is measured in the lab frame. The next step is to use these approximations, make a small angle approximation for $\cos\theta$ and drop terms of order m_π/m_D. This gives,

$$\Delta m = m_\pi + \frac{p_\pi^2}{2m_\pi}\theta^2. \tag{32}$$

In this picture one can see that most of the uncertainties associated with the D have canceled out; all that is left is the contribution of the D to the error on θ. Now, consider the specific example of the decay chain, $D^{*+} \to D^0\pi^+_{slow}$, followed by $D^0 \to K^-\pi^+$, as observed in the CLEO detector. The pion from the D^* decay is labeled π^+_{slow} because the kinematics of the decay constrain it to have a momentum below about 0.450 GeV. On the other hand, the two daughters of the D^0 typically have momenta in the range of 1.0 to 2.0 GeV. Because of their higher momentum, the D^0 daughters suffer much less multiple scattering and do not make a significant contribution to the error on the opening angle. Therefore the error on the opening angle is dominated by the multiple scattering component of the error on the direction of the slow π, which is on the order of 5 to 10 mr. For typical D^* candidates the opening angle is on the order of 50 mr. The error on the momentum of the slow π is on the order of a few percent. Therefore the error on the mass difference is dominated by the error on the opening angle, which is itself dominated by the error on the direction of the slow π^+.

The above is an illustration of a general rule, that, when the lab opening angle between two systems is very small, then the error on the invariant

Decay	BranchingFraction(%)
$D^0 \to K^-\pi^+$	4.01 ± 0.14
$D^0 \to K^-\pi^+\pi + \pi^-$	8.1 ± 0.5
$D^0 \to K^-\pi^+\pi^0$	13.8 ± 1.0
$D^0 \to K^0_S\pi^+\pi^-$	2.6 ± 0.3
$D^+ \to K^-\pi^+\pi^+$	9.1 ± 0.6
$D_s \to \phi\pi$	3.5 ± 0.4
$\Lambda_c \to pK^-\pi^+$	4.4 ± 0.6
$\Xi_c^+ \to \Xi^-\pi^+\pi^+$	2.1 ± 0.9

Table 10: Benchmark decay modes for some charmed hadrons. The scale of the branching fractions for the D_s, Λ_c and Ξ_c are poorly determined. All of the branching fractions are taken from the Review of Particle Properties [6], except that for the Ξ_c^+, which is taken from [54].

mass of the combined system is dominated by the error on the opening angle. Conversely, when the lab opening angle is close to 180°, then the error on the invariant mass of the combined system is dominated by the error on the magnitude of the momentum of each of system.

While the D^* trick works well in all detectors for the decay $D^{*+} \to D^0\pi^+$, the CLEO calorimetry is good enough that it also works for the decays $D^* \to D\pi^0$.

4.3 Benchmark Modes

The excited charmed mesons all eventually decay strongly or electromagnetically to one of the D^0, D^+ or D_s^+ mesons. Therefore any measurement of one of the excited states requires first reconstructing one of these three mesons. While these mesons have hundreds of decay modes, only two or three are used regularly. These are known as the benchmark modes and they are characterized by both a relatively large value of $\epsilon \cdot B$ and a relatively good signal to background ratio. Here ϵ is the overall efficiency to reconstruct the mode, including fiducial volume effects, and B is the branching fraction to the benchmark mode. The benchmark modes for the charmed mesons and for some of the charmed baryons are summarized in table 10.

The general quality of some of the benchmark modes for CLEO can be

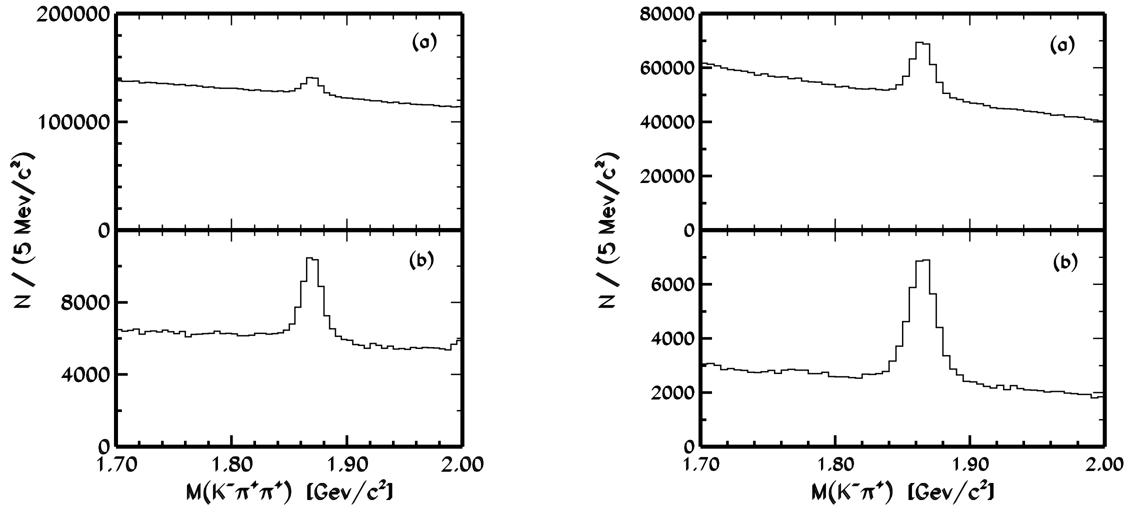

Figure 13: Benchmark D^+ and D^0 modes from CLEO. The left hand figure shows invariant mass spectra of $K^-\pi^+\pi^+$ combinations while the right hand figures shows spectra for $K^-\pi^+$ combinations. In both cases a) $x_p > 0.$ and b) $x_p > 0.6$.

seen in figures 13 and 14. For these figures, the particle identification criteria are as described in [55]. In the ARGUS detector the benchmark modes have a slightly poorer signal to background ratio, which is explained by the lower magnetic field. In the fixed target detectors the signal to background ratio for the D^+ is improved by about a factor of 15 while that for the D^0 is improved by about a factor of 2. The dramatic improvement for the D^+ is the result of its long lifetime which ensures a high efficiency for clean separation between the charm production and decay vertices. In each detector, the signal to background for the D_s benchmark modes is about the same as that for the D^0 mode in the same detector. At CLEO and ARGUS the benchmark Λ_c modes also have a signal to background ratio similar to that of the D^0 mode. At the fixed target experiments, the signal to background ratio for the D^* benchmark modes is slightly poorer than is shown here.

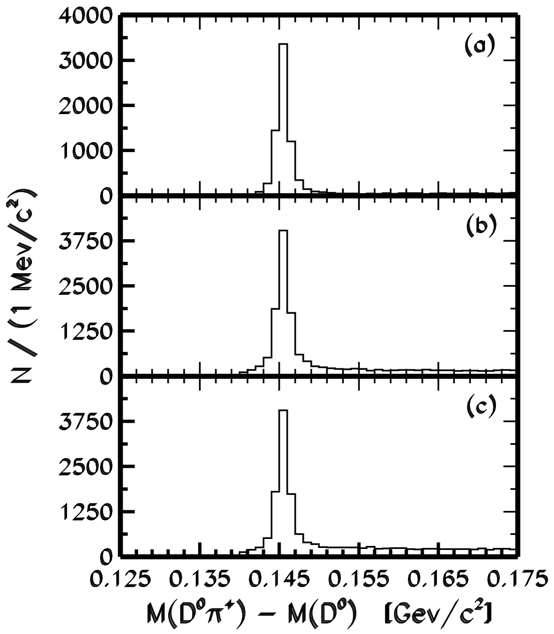

Figure 14: Benchmark $D^{*+} \to D^0\pi^+$ modes from CLEO; a) $D^0 \to K^-\pi^+$, b) $D^0 \to K^-\pi^+\pi^0$ and c) $D^0 \to K^-\pi^+\pi^+\pi^-$. All histograms are for $x_p > 0.6$.

5 More Experimental Results

5.1 Vector-Pseudoscalar Mass Splittings

In potential models the mass splitting between the vector and pseudoscalar mesons is due to the colour hyperfine interaction and the value of the splitting is given by,

$$\Delta M(^3S_1 -^1 S_0) \ \propto \ \frac{1}{m_Q m_q} \left|\psi(0)\right|^2 , \tag{33}$$

where $\psi(0)$ is the value of the wavefunction at the origin. The experimental data for several such splittings are summarized in Table 11. In the light hadron sector this formula worked well if one ignored the factor of $|\psi(0)|^2$ [10] and, therefore, the first predictions in the heavy flavour sector were made ignoring possible variations in $|\psi(0)|^2$. These predictions were that the splitting $M(D_s^*) - M(D_s)$ should be on the order of 100 MeV and early, but erroneous, experimental data seemed to confirm that [56]. However it is now firmly established that the correct splitting in the D_s sector is within a few MeV of

$Q\overline{q}$	States	Experiment (MeV)	$[M(D^*)-M(D)]\frac{m_c m_u}{m_Q m_q}$ (MeV)
$s\overline{u}$ $s\overline{d}$	$K^*(892)-K$	398.1 ± 0.3	385
$c\overline{u}$ $c\overline{d}$	$D^*(2010)-D$	141.4 ± 0.08	Input
$b\overline{u}$ $b\overline{d}$	$B^*(5325)-B$	46.0 ± 0.06	42
$c\overline{s}$	$D_s^*(2110)-D_s$	143.97 ± 0.41	90

Table 11: Vector-Pseudoscalar splittings for various heavy-light meson systems [6, 1]. The entries for the $I = 1/2$ states give the average of the two members of the multiplet. The third column presents the predictions of an early model. The reasons behind the successes and failures of that model are now understood.

that in the D sector. In the relativized quark model [16] this is understood to be a numerical accident — the change in the wavefunction at the origin almost exactly compensates for the change in the mass of the light quark. On the other hand, HQS suggests that $|\psi(0)|^2$ is the same in both the D and B sectors. This is borne out by the data.

The story of the first correct observation of the D_s^* is an example of an experimental *tour de force* [57]. Recall that the dominant decay mode of this state is $D_s^* \to D_s\gamma$. This discovery was made using the ARGUS detector which had, for its time, the most advanced electromagnetic calorimetry ever installed in a 4π magnetic spectrometer. In order to suppress backgrounds a high minimum energy cut was placed on the photon. However, this distorts the lower edge of the line shape and shifts the observed mass upwards. After a lot of work on the simulation of the response of the calorimeter, a correction of -12 ± 4 MeV was applied to the raw measured mass, giving a $D_s^* - D_s$ mass splitting of $144 \pm 9 \pm 7$ MeV. This compares well with the presently accepted value given in table 11.

State	$c\overline{s}$	$c\overline{d}$	Δm(MeV)
$^1S_0$	D_s^+	D^+	99.1 ± 0.6
$^3S_1$	D_s^{*+}	D^{*+}	$103.3 \pm 1.$
$P_1^{3/2}$	D_{s1}^+	D_1^+	$114 \pm 3.$
$P_2^{3/2}$	D_{s2}^{*+}	D_2^{*+}	$110 \pm 4.$
	$\overline{b}s$	$\overline{b}d$	
$^1S_0$	B_s^0	B^0	$96 \pm 6.$

Table 12: Mass differences of mesons which differ by the substitution of an s quark for a d quark. Most of the mass splittings are from [6], except for those of the P-wave mesons which are taken from [2]. The D_s^* mass also contains some information from [58, 1].

5.2 Substitution of an s Quark for a d Quark

In the light hadron sector a rough rule holds that substituting a strange quark for a light quark, while keeping everything else fixed, adds approximately 150 MeV to the mass of a hadron. Table 12 shows the corresponding comparison for the heavy flavour sector. Clearly the same effect is present, although the magnitude of the shift is somewhat less than in the light hadrons. The HQS prediction that the splitting $M(B_s) - M(B^0)$ should be the same as the splitting $M(D_s) - M(D^+)$ is upheld at the level of the present errors.

There are two splittings in the charmed baryon sector where one can make the same comparison, $M(\Xi_c^{*+}) - M(\Sigma_c^{*+})$ and $M(\Xi_c^{*0}) - M(\Sigma_c^{*0})$. At first thought, these comparisons cannot be made properly because only the Σ_c^{*++} and the Ξ_c^{*0} have been established. However the experimental uncertainty on the mass of the Σ_c^{*++} is much larger than the expected isospin mass splittings within the Σ_c^* multiplet. So one can add to the list of comparisons, $M(\Xi_c^0) - M(\Sigma_c^*) = 113 \pm 5$ MeV, which falls within the pattern seen in the meson sector.

Because of the mixing between the Ξ_c and the Ξ_c' one does not expect the same simple picture for $M(\Xi_c') - M(\Sigma_c)$ and $M(\Xi_c) - M(\Lambda_c)$. In fact one could use these splittings to learn about the magnitude of the mixing.

States	Splitting(MeV)
$M(D_2^{*+}) - M(D_1^+)$	34 ± 5 MeV
$M(D_2^{*0}) - M(D_1^0)$	37 ± 3 MeV
$M(D_{s2}^{*+}) - M(D_{s1}^+)$	38 ± 2 MeV

Table 13: Mass splittings with the $j_\ell = 3/2$ P-wave charm multiplets.

5.3 P-wave Charmed Meson Summary

As was discussed in section 3.1.2, there should be to be six P-wave charmed and charmed-strange mesons with $j_\ell = 3/2$. All of these have now been found and their masses have been well measured. They have been identified as the $j_\ell^P = 3/2^+$ mesons on the basis of the angular distributions in their decay and because their widths are on the scale of a few MeV to a few tens MeV, not on the scale of a few hundred MeV. More complete discussions of the J^P and j_ℓ assignments can be found in [55],[24], [59],[60]. A good summary of the status of the J^P assignments is that, while they are not rigorous, neither are they subject to any serious challenge [2].

Recently a review has been prepared which summarizes the current state of knowledge about the P-wave charmed and charmed strange mesons [2]. The authors have gone back to the original papers and corrected the results for improvements to the contributing measurements. For example, the reported masses have been corrected to incorporate new values of the D^* mass. Also world averages have been calculated using the methods specified by the Particle Data Group, including their method of calculating scale factors for errors. In general the experiments agree with each other well, the one problem being that there is some disagreement between ARGUS and CLEO on the total cross-sections and on the fragmentation functions.

The world average masses and widths computed in [2] have been summarized in figures 15, 16 and 17, and in table 13. Here the agreement of the data between experiments is fine. However, in the non-strange sector, the world average width measurements still have fairly large errors. These errors are large because of several effects in the backgrounds. First, because the signals sit on the top of a broad bump in the background, the measured width is strongly correlated with the background shape. Second, the background shapes are not well known and they contain many regions which are contam-

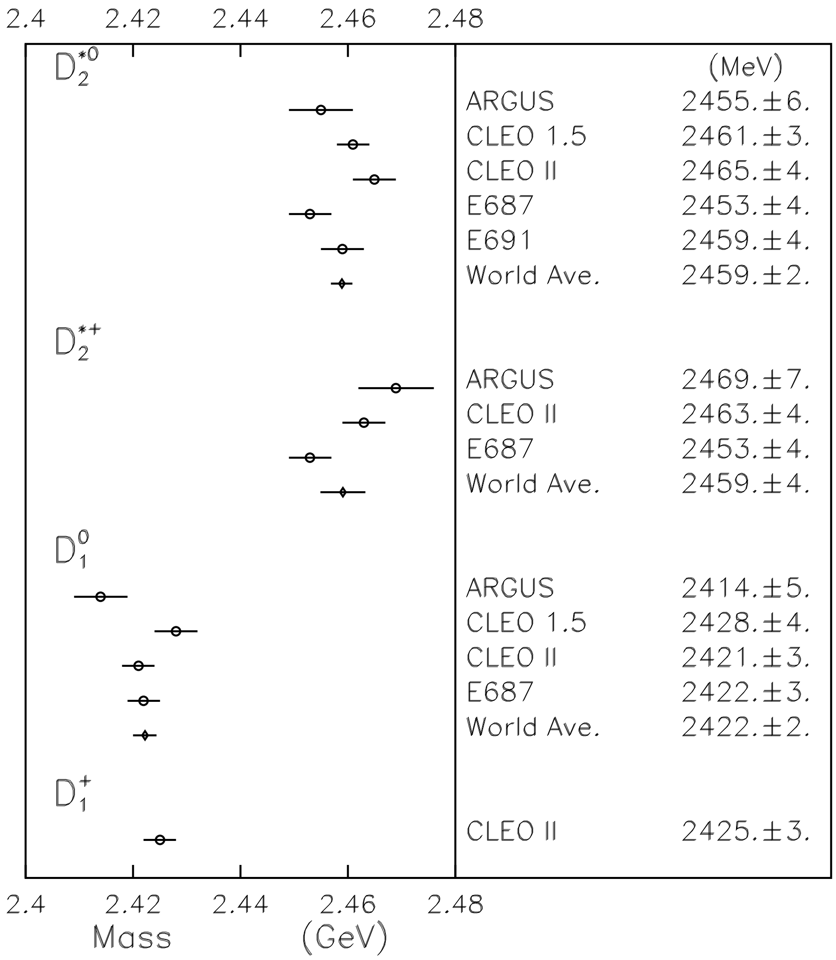

Figure 15: Masses of P-wave charmed mesons, from [2].

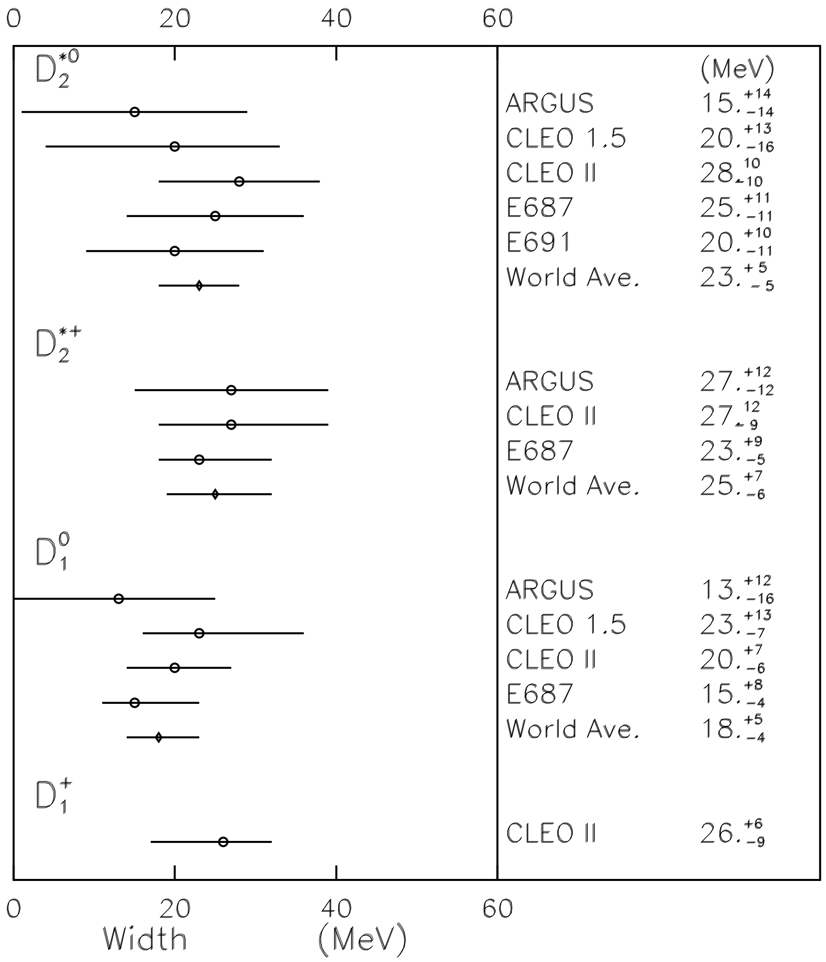

Figure 16: Widths of P-wave charmed mesons, from [2].

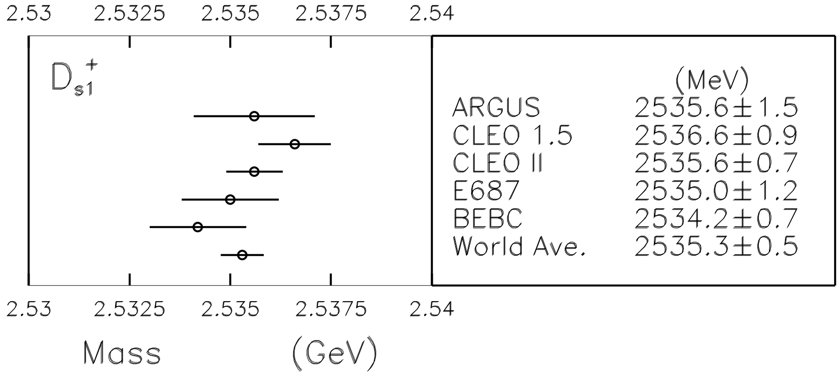

Figure 17: Measurements of the mass of the D_{s1}^{+} meson, from [2]. The state has a width of $\Gamma \leq 2.3$ MeV @ 90% C.L.. The $J^P = 2^+$ partner has a mass of $2573. \pm 2$ MeV and a width of 16 ± 2 MeV.

inated by feed down from and reflections of other P-wave charmed mesons. Taken together these effects cause a poor determination of the widths. Moreover there are few immediate prospects for improvement. For example, most of the background in the $D^{*+}\pi^-$ final state is due to real D^{*+} candidates combined with fragmentation pions. That is, the background is from physics and cannot be removed by upgraded detectors.

One of the interesting distributions in the decay of the P-wave charmed mesons is that of the helicity angle. In the decay chain, $D_1 \to D^*\pi_1$, $D^* \to D\pi_2$, the helicity angle, α, is defined as the angle between the direction of π_2 and the direction of π_1, when both are measured in the rest frame of the D^*. It is defined similarly for the decay $D_2^* \to D^*\pi$. Figure 18 shows measured distributions of $\cos\alpha$ for the decays of the D_2^* and the D_1 [55]. Assuming that the D_2 does indeed have $J^P = 2^+$, the shape of the distribution in part a) must be proportional to $\sin^2\alpha$ and the data are consistent with that shape.

Assuming that the D_1 does indeed have $J^P = 1^+$, the shape of the distribution in part b) depends on the partial wave amplitudes, S and D, in the decay of the D_1. In the limit that the decay takes place in a pure D-wave, the expected shape of the distribution is $(1 - 3\cos^2\alpha)$, and the data are consistent with that shape. However this is not sufficient evidence to conclude that the ratio $|S|/|D|$ is small — one must consider the interference between the two partial waves. Following [55] the general form of the distribution is

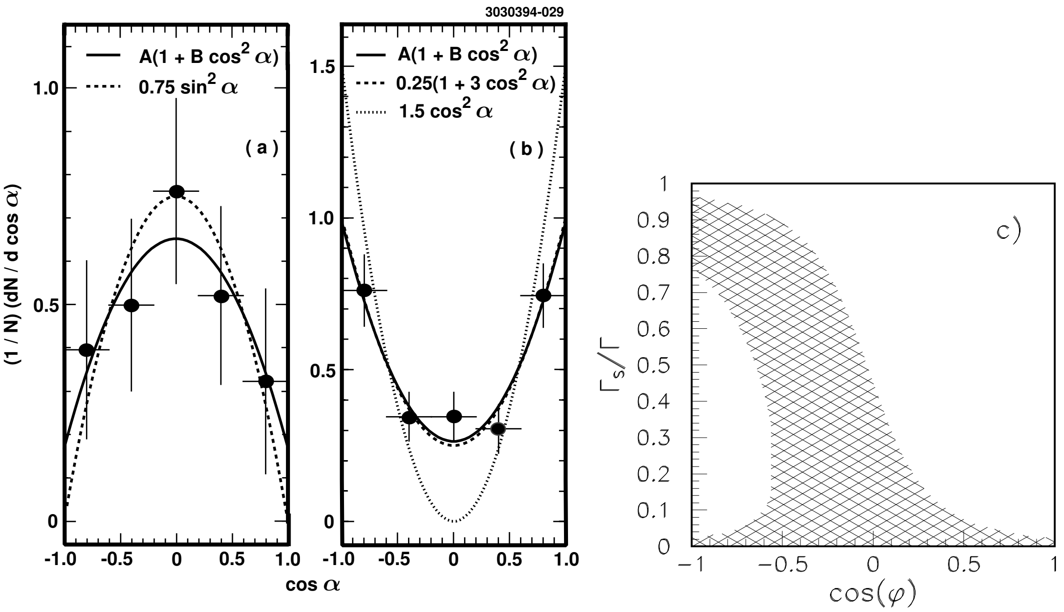

Figure 18: The measured distributions of $\cos\alpha$ for the decays a) $D_2^*(2460)^0 \to D^{*+}\pi^-$ and b) $D_1(2420)^0 \to D^{*+}\pi^-$. The superimposed curves are described and interpreted in the paper from which the data are taken [55]. For the decay of the D_1^0, part c) shows the allowed region in plane of Γ_S/Γ vs φ. The notation is defined in the text.

written in terms of the variables R and φ, defined by, $\Gamma_S = |S|^2$, $\Gamma_D = |D|^2$, $\Gamma = \Gamma_S + \Gamma_D$, $R = \Gamma_S/\Gamma$ and $\varphi = \arg(S^* D)$. In terms of these variables, the shape of the angular distribution is,

$$\frac{dN}{d\cos\alpha} \propto R + (1-R)\frac{1+3\cos^2\alpha}{2} + \sqrt{2R(1-R)}\cos\varphi\left(1-3\cos^2\alpha\right) \quad (34)$$

Clearly many different values of R and φ can lead to a $\cos\alpha$ distribution with the observed shape. Figure 18c) shows the region in the R-φ plane which, at the 90% C. L., is allowed by the data in figure 18b). Therefore R is actually quite poorly constrained by the data.

At present the theoretical calculations of the partial wave amplitudes have been done in the Born approximation, in which the S and D are both real. If one believes that this is correct then R is constrained to be quite small. On the other hand, if one allows a relative phase between the amplitudes, then the theory gives no guidance about how to constrain R. Conversely, table 9 shows that the prediction of R is quite uncertain, which means that figure 18c) cannot be used to constrain ϕ.

There are two speculations which have been advanced about figure 18 parts b) and c). The first speculation is an Occam's razor approach. If there is a substantial S-wave amplitude, then it must be an accident that the shape in b) agrees so well with the limit that there is no S-wave. People who do not believe in accidents can then argue that the S-wave component must be small. The second speculation was advanced by Falk and Peskin [61]. They start with equation 18 and introduce phase space factors of p^{2L+1}. Next, they recognize that, for small mixing angles, $\sin(\phi-\phi_0) = (\phi-\phi_0)$ while $\cos(\phi-\phi_0) = 1$. Therefore, to first order in the mixing angle, these equations predict, with no free parameters, the D-wave partial width of the D_1 in terms of the total width of the D_2^*. Using their method and $\Gamma(D_2^0) = 23\pm5$ MeV [2] gives the prediction $\Gamma_D(D_1) = 6.2 \pm 1.4$ MeV, which is about 3 standard deviations from the measured total width of the D_1, 18^{+5}_{-4} MeV [2]. Taken at face value, this suggests that the S-wave partial width of the D_1 is larger than its D-wave partial width.

It is formally straightforward to resolve the question about the S-wave to D-wave ratio in these decays. One needs to consider three angles. The first angle is α and the other two are θ and χ, defined below. In the above decay chain, θ is the angle between the direction of the π_1 and the direction of the lab frame, when both are measured in the rest frame of the D_1. And χ is the angle between the production and decay planes of the D^*, measured in the rest frame of either the D^* or the D_1. By looking at various projections of the distributions in these angles one can disentangle R, φ and ρ_{00}. This last variable is the fraction of D_1 mesons with helicity zero, as measured in the lab frame. It may be possible to obtain a significant result with the existing data and it will certainly be possible when several times more data is available.

6 The future

Over the next 10 years, there will be many advances in heavy flavour spectroscopy, particularly in charm spectroscopy. For example, many of the existing CLEO results used only 40% to 60% of their final data sample. Updates and new results will be forthcoming as the final data set is passed through the main track reconstruction program. Similarly, WA89 and E687 have not yet published final results on all of their data. In October 1995, CLEO will begin taking a new data set, for which the innermost tracking system will be replaced by a silicon microstrip detector. This represents a substantial upgrade, particularly for decays involving the long-lived D^+.

In the longer term, three B-factories are under construction, BaBar at SLAC, Belle at KEK and CLEO III at Cornell. Because these experiments will focus on weak decays of B mesons produced in the decays of the $\Upsilon(4S)$, they will not contribute to b hadron spectroscopy. However, in the next 10 years, each of these experiments will reconstruct more than 20 times as many charmed hadrons as have been reconstructed to date. Moreover these decays will be observed using detectors which are better than the existing ones. Not only will the existing states be measured more precisely but many of the missing states will be observed. For example, the $j_\ell = 1/2$ P-wave charmed mesons, which are expected to be very broad, will be observed in the Dalitz plots of the decays $B \to D\pi\pi$ and $B \to D^*\pi\pi$. There is also some hope for seeing the broad D_s P-wave states by looking in at the Dalitz plots for $B \to D^{(*)}\overline{D}^{(*)}K$. There are excellent prospects for finding the missing singly charmed S-wave baryons. Some of the P-wave charmed baryons are expected to have widths on the order of tens of MeV and these should also be observable. The subjects which show little promise are to observe states with more than one unit of orbital angular momentum between the quarks or states with more than one heavy flavour, such as $b\overline{c}$ or ccq.

In a few years there will be another run of the Fermilab fixed target program, with excellent prospects for new contributions to charm spectroscopy. Any future runs of the CERN fixed target program are also likely to produce new results.

The near term future of bottom hadron spectroscopy also looks good. Preliminary results from LEP show indications of signals for the P-wave $b\overline{q}$ and $b\overline{s}$ mesons and there is some indication of the Σ_b and the Σ_b^*. Also the hadron collider groups are working hard to observe the P-wave B mesons to use as flavour tags in $B\overline{B}$ mixing and CP violation studies. Almost certainly the signals are there, and, with the help of silicon microstrip detectors, there is some hope of seeing them. On the down side, the LEP program will likely be cut short before accumulating enough luminosity to make much progress in the bottom baryon sector. Finally, the longer term status depends on how well the current program at the hadron colliders succeeds. There are plenty of bottom hadrons around, but they are usually accompanied by large backgrounds.

7 Acknowledgments

I would like to thank David Bugg for inviting me to speak at this institute, and for putting up with my tardiness in preparing these proceedings. He and the other organizers provided us all with the wonderful experience of discussing interesting physics, at a comfortable pace and in pleasant surroundings. The other speakers did a wonderful job of opening my eyes to several areas of physics which I have not had the opportunity to follow over the years. Finally, I would also like to thank the students for their questions which help to keep the field exciting.

References

[1] CLEO II Collab., J. Gronberg *et al.*, Preprint CLNS 95/1346,CLEO 95-10,EPS0177, CLEO (unpublished).

[2] J. Bartelt and S. Shukla, Ann. Rev. Nucl. Part. Sci. **45**, 83 (1995).

[3] CLEO II Collab., P. Avery *et al.*, Preprint CLNS 95/1352,CLEO 95-14,EPS0172, CLEO (unpublished).

[4] E. Chudakov, talk at the Conference on Heavy Quarks at Fixed Targets, Virgina, 1994.

[5] CLEO II Collab., K. W. Edwards *et al.*, Phys. Rev. Lett. **74**, 3331 (1995).

[6] Particle Data Group, Phys. Rev. **D50**, 1173 (1994).

[7] M. K. Gaillard, B. W. Lee, and J. L. Rosner, Rev. Mod. Phys. **47**, 277 (1975).

[8] CLEO II Collab., F. Butler *et al.*, Phys. Rev. Lett. **69**, 2041 (1992).

[9] N. Isgur, in *The New Aspects of Subnuclear Physics; Proceedings of the XIV International School of Subnuclear Physics*, edited by A. Zichichi (Plenum, New York, 1978).

[10] F. E. Close, *An Introduction to Quarks and Partons* (Academic Press, New York, 1979).

[11] A. Rújula, H.Georgi, and S. Glashow, Phys. Rev. **D12**, 147 (1975).

[12] W. Kwong, J. L. Rosner, and C. Quigg, Ann. Rev. Nucl. Part. Sci. **37**, 325 (1987).

[13] K. Wilson, Phys. Rev. **D10**, 2445 (1974).

[14] J. Kogut and L. Susskind, Phys. Rev. **D9**, 3501 (1974).

[15] T. Barnes, private communication.

[16] S. Godfrey and N. Isgur, Phys. Rev. **D32**, 189 (1985).

[17] S. Capstick and N. Isgur, Phys. Rev. **D34**, 2809 (1986).

[18] J. Rosner, Comm. Nucl. Part. Phys. **16**, 109 (1986).

[19] N. Isgur and G. Karl, Phys. Rev. **D18**, 4187 (1978).

[20] S. Godfrey and R. Kokoski, Phys. Rev. **D43**, 1679 (1991).

[21] ARGUS Collab., H. Albrecht *et al.*, Phys. Rev. Lett. **56**, 549 (1986).

[22] ARGUS Collab., H. Albrecht *et al.*, Phys. Lett. **230B**, 162 (1989).

[23] E691 Collab., J.C. Anjos *et al.*, Phys. Rev. Lett. **62**, 1717 (1989).

[24] CLEO II Collab., T. Bergfeld *et al.*, Phys. Lett. **340B**, 194 (1994).

[25] N. Isgur and M. Wise, Phys. Lett. **232B**, 113 (1989).

[26] N. Isgur and M. Wise, Phys. Lett. **237B**, 527 (1990).

[27] R. Barbieri *et al.*, Nucl. Phys. **B105**, 125 (1976).

[28] D. Pignon and C. Piketty, Phys. Lett. **81B**, 334 (1979).

[29] E. Eichten *et al.*, Phys. Rev. **D21**, 203 (1980).

[30] J. Morishita *et al.*, Phys. Rev. **D37**, 159 (1988).

[31] V. Gupta and R. Kögerler, Zeit. Phys. **C41**, 277 (1988).

[32] A. Kaidalov and A. Nogteva, Sov. J. Nucl. Phys. **47**, 321 (1988).

[33] K. Maltman and N. Isgur, Phys. Rev. **D22**, 1701 (1980).

[34] L. A. Copley, N. Isgur, and G. Karl, Phys. Rev. **D20**, 768 (1979).

[35] J. M. Richard and P. Taxil, Phys. Lett. **128B**, 453 (1983).

[36] ARGUS Collab., H. Albrecht *et al.*, PL **317B**, 227 (1993).

[37] E687 Collab., P. L. Frabetti *et al.*, Phys. Rev. Lett. **72**, 961 (1994).

[38] L. Micu, Nucl. Phys. **B10**, 521 (1969).

[39] A. L. Yaouanc *et al.*, Phys. Rev. **D8**, 2223 (1973).

[40] A. L. Yaouanc *et al.*, Phys. Rev. **D9**, 1415 (1974).

[41] A. L. Yaouanc *et al.*, Phys. Rev. **D8**, 2223 (1973).

[42] J. P. Ader *et al.*, Zeit. Phys. **C5**, 85 (1980), note: Equation (12) has L_A and S_A interchanged.

[43] R. Kokoski and N. Isgur, Phys. Rev. **D35**, 907 (1987).

[44] E. J. Eichten, C. T. Hill, and C. Quigg, Phys. Rev. Lett. **71**, 4116 (1993).

[45] N. Isgur and M. Wise, Phys. Rev. **D66**, 1130 (1991).

[46] A. F. Falk and M. Luke, PL **292B**, 119 (1992).

[47] P. Cho and S. P. Trivedi, PR **D50**, 381 (1994).

[48] Particle Data Group, Phys. Rev. **D45**, S1 (1992).

[49] CLEO II Collab., D. Bortoletto *et al.*, Phys. Rev. Lett. **69**, 2046 (1992).

[50] P. Cho and M. B. Wise, PR **D49**, 6228 (1994).

[51] ARGUS Collab., H. Albrecht *et al.*, Nucl. Instr. Methods **A275**, 1 (1989).

[52] CLEO II Collab., Y. Kubota *et al.*, Nucl. Instr. Methods **A320**, 66 (1992).

[53] B. Andersson *et al.*, Phys. Rep. **97**, 31 (1983).

[54] CLEO II Collab., J. Alexander *et al.*, Phys. Rev. Lett. **74**, 3113 (1995), the number quoted in the text comes from an erratum which has been submitted to Phys. Rev. Lett.

[55] CLEO II Collab., P. Avery *et al.*, Phys. Lett. **331B**, 236 (1994).

[56] R. Brandelik *et al.*, PL **70B**, 132 (1977).

[57] ARGUS Collab., H. Albrecht *et al.*, PL **146B**, 111 (1984).

[58] CLEO II Collab., D. N. Brown *et al.*, Phys. Rev. **D50**, 1884 (1994).

[59] CLEO II Collab., Y. Kubota *et al.*, Phys. Rev. Lett. **72**, 1972 (1994).

[60] CLEO II Collab., J. P. Alexander *et al.*, Phys. Lett. **303B**, 377 (1993).

[61] A. F. Falk and M. E. Peskin, PR **D49**, 3320 (1994).